NASA TECHNICAL MEMORANDUM

UB
NASA TM X-1994

HYPERSONIC AERODYNAMIC CHARACTERISTICS OF DL-4 LIFTING ENTRY VEHICLE

by Charles L. Ladson
Langley Research Center
Langley Station, Hampton, Va.

NATIONAL AERONAUTICS AND SPACE ADMINISTRATION • WASHINGTON, D. C. • APRIL 1970

C70-591

CONFIDENTIAL

1. Report No.	2. Government Accession No.	3. Recipient's Catalog No.
NASA TM X-1994		

4. Title and Subtitle	5. Report Date
HYPERSONIC AERODYNAMIC CHARACTERISTICS OF DL-4 LIFTING ENTRY VEHICLE [redacted]	April 1970
	6. Performing Organization Code
7. Author(s)	8. Performing Organization Report No.
Charles L. Ladson	L-6592
	10. Work Unit No.
9. Performing Organization Name and Address	124-64-02-03-23
NASA Langley Research Center Hampton, Va. 23365	11. Contract or Grant No.
	13. Type of Report and Period Covered
12. Sponsoring Agency Name and Address	Technical Memorandum
National Aeronautics and Space Administration Washington, D.C. 20546	14. Sponsoring Agency Code

15. Supplementary Notes

16. Abstract

Aerodynamic forces on a representative, high-performance, entry configuration with a lift-drag ratio of about 3 have been obtained at Mach numbers of 6 and 10 in air and 20 in helium. These data are compared with theory to identify areas in which the theoretical methods are adequate and the areas in which improvement is necessary. Experimental results of Mach 10 tests of tip-fin and body modifications are also presented to show the attempts that have been made to develop a configuration which is stable about all axes.

17. Key Words (Suggested by Author(s))	18. Distribution Statement
Lift-drag ratio of about 3 class Hypersonic data Aerodynamic force data Lifting entry vehicle	[redacted]

19. Security Classif. (of this report)	20. Security Classif. (of this page)	21. No. of Pages	22. Price
[redacted]	[redacted]	44	

HYPERSONIC AERODYNAMIC CHARACTERISTICS OF DL-4 LIFTING ENTRY VEHICLE*

By Charles L. Ladson
Langley Research Center

SUMMARY

A comparison of theoretical and experimental force data at speeds from a Mach number of 6 to a Mach number of 20 has been made on a lifting entry vehicle with a hypersonic lift-drag ratio of about 3. The results indicate that although normal force can be predicted rather well, the lift-drag ratio is overpredicted by as much as 0.7. The experimental center of pressure was consistently forward of the theoretical location although the forward movement with increasing Mach number was adequately predicted. Directional and lateral stability parameters could not be calculated reliably.

Experimental results at a Mach number of 10 indicate that the basic body shape has a maximum untrimmed lift-drag ratio of about 3.2 but is longitudinally and directionally unstable throughout the test angle-of-attack range with a region of lateral instability at the lower angles of attack. Addition of an undeflected elevon and a tip fin rolled out 20° and toed in 5° resulted in a configuration which trims at a lift-drag ratio of about 2.9 and is directionally and laterally stable above an angle of attack of about 4°. By use of aft body modifications in place of discrete tip fins, the vehicle trimmed at a lift-drag ratio of 2.8, was directionally stable at positive angles of attack, but was laterally unstable below the angle of attack for maximum lift-drag ratio.

INTRODUCTION

For the past several years, considerable attention at the Langley Research Center has been focused on the development of spacecraft configurations designed for decoupled landing. Some of these concepts utilizing the decoupled mode are reviewed in reference 1, and details of the application of propulsive lift and decoupled rotor are presented in references 2 and 3, respectively. As indicated in reference 1, vehicles with hypersonic maximum lift-drag ratios of about 1 to 3 have been considered.

The present investigation was conducted for the following reasons: first, to determine a basic vehicle shape which would be typical of the vehicles with a hypersonic

maximum lift-drag ratio of about 3; second, to obtain experimental hypersonic aerodynamic characteristics of this basic shape and to compare them with theory so that the adequacy of the theory can be determined; and third, to provide the basic vehicle shape with stability about all axes by means of appropriate modifications.

This paper presents the aerodynamic characteristics of a basic vehicle shape (designated DL-4A) at Mach numbers of 6 and 10 in air and 20 in helium over a range of Reynolds numbers. Results of these six-component force data are presented and compared with theory to expose those areas in which the differences between existing theory and experiment are the greatest. Force tests were also conducted at a Mach number of 10 on the basic body shape with various orientations of tip fins and on a modified body shape without tip fins to provide an indication of the directional and lateral stability characteristics which can be expected on this class of vehicle.

The Mach 6 data, obtained in the Langley 20-inch hypersonic tunnel, were provided by George C. Ashby, Jr., and the Mach 20 data, obtained in the Langley 22-inch helium tunnel, were provided by James P. Arrington who also performed the theoretical analysis. The Mach 10 data were obtained in the Langley continuous-flow hypersonic tunnel.

SYMBOLS

b	model span
C_A	axial-force coefficient, $\frac{\text{Axial force}}{qS}$
C_D	drag coefficient, $\frac{\text{Drag}}{qS}$
C_L	lift coefficient, $\frac{\text{Lift}}{qS}$
C_l	rolling-moment coefficient, $\frac{\text{Rolling moment}}{qSb}$
C_{l_β}	lateral stability parameter
C_m	pitching-moment coefficient, $\frac{\text{Pitching moment}}{qSl}$
C_N	normal-force coefficient, $\frac{\text{Normal force}}{qS}$
C_n	yawing-moment coefficient, $\frac{\text{Yawing moment}}{qSb}$
C_{n_β}	directional stability parameter

C_Y side-force coefficient, $\frac{\text{Side force}}{qS}$

C_{Y_β} side-force damping derivative

L/D lift-drag ratio

l model reference length

M Mach number

q dynamic pressure

R Reynolds number based on model length

S projected planform area

x_{cp} longitudinal location of center of pressure

α angle of attack

β angle of sideslip

ϵ fin toe-in angle; angle between model vertical plane of symmetry and fin outer surface measured in horizontal reference plane of model (positive toe-in angle denotes trailing edge deflected away from vehicle center line)

ϕ fin roll-out angle; angle between model vertical plane of symmetry and fin outer surface measured in a plane normal to fin outer surface and vehicle lower surface (positive roll-out angle denotes fin outer surface rolled outboard of vertical)

MODELS

The basic body shape, designated DL-4A (fig. 1), has a highly swept planform and a trapezoidal cross section. A cambered lower surface provides a positive incremental pitching moment, and the sloped sides canted inward reduce the local pressure and heating. Side modifications aft of the $0.75l$ station contribute an increment of C_{n_β}. The upper surface aft of the canopy is flat to provide for a deployable landing system (such as a deployable wing). From preliminary internal layouts of a 50-foot (15.24-m) vehicle, a

center-of-gravity location of 0.61ℓ behind the nose and 0.01ℓ below the reference axis was selected for the moment reference center. The configuration is not presented as an optimum design but, rather, as a representative L/D = 3 design which would expose typical problem areas for which general solutions could be explored.

Tip fins and a center-line vertical tail having areas of 15 and 10 percent of the model reference area (fig. 2), respectively, were also tested. Five combinations of tip-fin toe-in and roll-out angles were tested on the vehicle designated DL-4F. Two modifications of the aft end of the vehicle (fig. 2) were made to provide directional stability without use of discrete fins. One modification consisted of a ramp partially blending the highly swept tip fin into the body. The ramp provides a positive pitching-moment increment at zero lift. The second modification (DL-4G) consisted of blending the same highly swept fin leading edge into the body upper surface; thus, the ramp surface of the previous modification is eliminated. Both of these blended fin-body configurations were designed to reduce the fin leading-edge heating problem and any fin-body interference problems which might exist. Photographs of the small basic-body model and the large steel model with tip fins are shown in figure 3(a) and the two modified configurations, in figure 3(b).

All coefficients are based on the total projected planform area, the span, and the actual length of the model. The reference area and lengths for the two model sizes are as follows:

S		b		ℓ	
in^2	cm^2	in.	cm	in.	cm
24.98	161.16	3.354	8.52	12.60	32.00
156.1	1007.09	8.375	21.27	31.50	80.01

APPARATUS, TESTS, AND PROCEDURE

The data contained herein were obtained in three different facilities to cover the Mach number range from 6 to 20. The facilities, Mach numbers, Reynolds numbers, dynamic pressures, and model lengths are listed in table I, and the facilities are described in greater detail in reference 4.

Six-component electrical strain-gage balances were used to obtain the force and moment data. The model base pressure was measured in all tests, and the axial-force data have been adjusted to correspond to free-stream static pressure over the entire model base.

All longitudinal performance data are referred to the stability-axis system, whereas the stability results are referred to the body-axis system. All directional and lateral

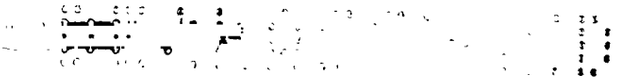

stability data at a Mach number of 6.0 in air and 20 in helium were obtained from tests at sideslip angles of 0° and about 5°. At a Mach number of 10, the data were obtained at sideslip angles from -4° to 8°. Inasmuch as the data were linear with β, only the slopes have been presented.

Balance accuracy based upon the static calibrations is presented in table II in terms of the aerodynamic coefficients. The accuracy for the angles of attack and sideslip was within $\pm 0.2^{\circ}$, and the accuracy in Mach number was ± 0.02 at a Mach number of 6, ± 0.05 at a Mach number of 10.3, and ± 1 percent at a Mach number of 20 for the helium tests.

RESULTS AND DISCUSSION

Comparison of Theoretical and Experimental Results for the Basic Body

Theoretical estimates of the aerodynamic force characteristics of the basic body were made by using an available digital computer program. Inviscid calculations were made by using tangent-cone theory for the windward surfaces, Newtonian theory for the spherical nose cap, and Prandtl-Meyer expansion from free-stream conditions for the Newtonian "shadow" regions of the vehicle. Laminar skin friction was calculated for all Mach numbers by using the reference-temperature method. Boundary-layer induced pressures were also calculated for the Mach 20 test conditions where these effects might become significant. Although this theoretical approach is relatively simple for such a complex vehicle shape, it was made in an attempt to show areas in which the theory could adequately predict results as well as areas in which it is inapplicable.

The comparisons of the measured normal- and axial-force coefficients with theory are presented in figure 4 for the three Mach numbers and various Reynolds numbers. In general, normal force is predicted well by the theory at the lower angles of attack but is slightly overpredicted at the higher angles of attack of the tests. Axial force is underestimated at all Mach numbers for both the highest and lowest test Reynolds numbers. The error in the prediction of axial force probably lies in the skin-friction calculations since the inviscid normal force was reasonably predicted. The possibility that the experimental boundary layer was transitional or turbulent, especially at the highest Reynolds number and low Mach number, may also have contributed to the higher axial force. Differences between theoretical and measured lift and drag coefficients (fig. 5) reflect the differences observed in C_N and C_A.

The lift-drag ratio and pitching-moment coefficients are shown in figure 6. The calculated maximum L/D is 0.3 to 0.7 higher than the measured ratio, but the variations with Mach number and Reynolds number follow the theory. The pitching-moment curves show the basic body to be longitudinally unstable (for the selected moment reference center) as predicted by the theory and also show large differences in the magnitude of the

theoretical and experimental values of the moment. The importance of this difference between theory and experiment is perhaps better expressed in terms of differences in center of pressure. (See fig. 7.) At a near-constant value of Reynolds number, the experimental center of pressure moves forward on the vehicle with increasing Mach number as the theory predicts but always lies forward of the theoretical value. The dependence upon angle of attack is also greater than that predicted. Although not predicted by the theory, some viscous effects are evident in the experimental data at the highest Mach number; the forward shift in center of pressure probably results from the higher induced pressure in the nose region.

The directional and lateral stability parameters are presented in figure 8. The measured values of the lateral stability parameter C_{l_β} are predicted fairly well at low angles of attack, but, at the higher angles shown, the measured values are negative where theory indicates a positive value for all Mach numbers. Unpublished pressure data on this vehicle at a Mach number of 10.4 show a lateral pressure gradient across the flat lower surface of the yawed model in the direction of the difference between theory and experiment. Theory does not predict any viscous effects on this parameter, but some variations with Reynolds numbers are observed experimentally at the highest Mach number. It should also be noted that the basic body is laterally unstable at low angles of attack, but the region of instability decreases with increasing Mach number.

With regard to the directional stability parameter C_{n_β}, theory does not predict the magnitude or the trends of the data with angles of attack, the largest differences being noted at the low angles of attack at a Mach number of 20. Again, the difference is attributed to the large induced pressure at the high Mach number which is not accounted for in the theory. The experimental data show essentially the same trends and magnitude for the two lower Mach numbers in air. It should also be noted that the basic body shape is directionally unstable at all test conditions. The side-force derivative C_{Y_β} is also shown in figure 8 and is slightly greater than that predicted by theory.

Effects of Various Model Components and Body Modifications (Mach 10)

Although theory and experiment indicate different degrees of instability, both show the basic body (DL-4A) to be generally unstable about all three axes for the assumed moment reference center. To provide a stable configuration, several fin arrangements and body modifications were investigated at a Mach number of 10. The effects of these modifications at a Reynolds number of about 4.7×10^6 are presented in the final part of this paper, and only a brief discussion of the principal results is presented.

Effects of elevon addition.- Since the basic body shape was longitudinally unstable, aft elevons and an elevon extension (fig. 1) were added to provide a vehicle shape which trims at an angle of attack near the maximum lift-drag ratio. The results (fig. 9) show

that the vehicle with the elevon undeflected is unstable below about 6° but is stable at the higher angles of attack and trims at about 12° or slightly above that for maximum L/D. The elevon decreases the maximum L/D by 0.2 but has no effect on the directional and lateral stability characteristics (fig. 9(c)).

Effects of tip-fin toe-in.- The experimental results of the effects of the addition of tip fins and variations of the toe-in angle ϵ at a near-constant value of roll-out angle ϕ are presented in figure 10. Both the addition of the fins to the basic body (DL-4A) with elevons and increases in the toe-in angle from 5.0° to 9.3° result in increases in both lift and drag coefficients (fig. 10(a)) with the net loss in maximum lift-drag ratio from 3.2 for the basic body to 2.5 for the maximum toe-in angle (fig. 10(b)). Addition of the fin with 5° toe-in angle results in a positive incremental pitching moment at angles of attack below about 5° and a negative increment above this angle. Increases in toe-in angle beyond 5° result in negative incremental pitching moments when compared with that for $\epsilon = 5^{\circ}$. (See fig. 10(b).) It is also interesting to note that the configuration with 5° toe-in angle trims at its maximum lift-drag ratio (about 2.9) with no elevon deflection.

Addition of the tip fins produces large positive increments in directional stability, the increment increasing with angle of attack as would be expected because of the larger flow deflection angle of the fin with respect to the free stream. (See fig. 10(c).) Increases of fin toe-in angle from 5° to 9.3° provide positive incremental increases in lateral stability for all angles of attack. The configuration with 5° toe-in is directionally and laterally stable above an angle of attack of about 4°.

Effects of tip-fin roll-out.- The experimental results of the effects of addition of tip fins and variation of the roll-out angle of the fins at a near-constant value of toe-in angle are presented in figure 11. The increases in lift and drag as well as the loss in maximum lift-drag ratio are essentially the same as were observed in figure 10 for the variations in toe-in angle. (See fig. 11(b).) Likewise, the negative out-of-trim incremental pitching moments due to increased roll-out angle are similar to the results of increased toe-in angle, but the increments are much larger because of the increased projected area of the vehicle aft of the moment reference center. For the roll-out angle of 0.4°, the vehicle trims at its maximum lift-drag ratio of about 2.9.

Figure 11(c) shows that addition of the fins at both 0.4° and 19.1° roll-out angle makes the vehicle directionally stable above an angle of attack of about 0°. For the extreme roll-out angle of 45°, the level of $C_{n_{\beta}}$ is reduced to about that for the 0.4° roll-out angle. Addition of the fin with near 0° roll-out has little effect on the lateral stability parameter but increases in roll-out angle generally produce large negative increments in this parameter, and for the highest roll-out angle, the vehicle is laterally stable for all positive angles of attack. (See fig. 11(c).)

These results for the variation of roll-out angle (fig. 11) must be taken qualitatively, however, since the toe-in angle was not constant at 7.5° as designed but was 6.6° and 8.0° for the two higher roll-out angles. By assuming that the trends of C_{l_β} and C_{n_β} shown in figure 10 also hold at the higher roll-out angle of 45°, the levels of these parameters for a constant toe-in angle of 7.5° could be estimated.

Effects of aft body modifications.- To avoid severe fin-body interference and high local heating, which may be present with discrete fin-body installations, the aft end of the basic body was modified to provide for directional stability without tip fins. Two modifications were made to the basic body (DL-4A), as shown in figures 2 and 3(b). The fully blended vehicle has been designated as DL-4G. Both of the body modifications increased the drag with little effect on the lift in the region of maximum lift-drag ratio (figs. 12(a) and 12(b)) and provided a longitudinally stable vehicle which trims at a lift-drag ratio of about 2.8. Measured pressure distributions over the upper surface of these configurations revealed an increase in pressure on the upper side surfaces of the blended vehicle as compared with the basic body. This pressure results in the large positive values of pitching moment obtained at an angle of attack of 0° as well as the large positive increment in C_{l_β} observed in figure 12(c). With the use of this aft body modification, the configuration trims at a maximum lift-drag ratio of 2.8, is both longitudinally and directionally stable, but is laterally unstable at angles of attack below that for maximum lift-drag ratio.

Effects of vertical tail.- Several previous studies have shown center-line vertical tails to be useful in increasing the directional stability of lifting bodies at low angles of attack (where the tail is not shielded from the flow). A low-aspect-ratio vertical tail (fig. 2) was added to the DL-4F configuration (with $\phi = 20°$ and $\epsilon = 5°$), and the results are shown in figure 13. These results show that the vertical tail reduces the maximum untrimmed L/D by about 0.2 with only a slight change in trim angle of attack. Substantial gains in both directional and lateral stability are observed at low angles of attack, but the tail becomes ineffective at an angle of attack of about 10° as would be expected.

Center-of-pressure variations.- The longitudinal locations of the center of pressure for the various configurations tested are presented in figure 14. These data are presented for information only and are not discussed.

CONCLUDING REMARKS

A comparison of theoretical and experimental force data at speeds from a Mach number of 6 to a Mach number of 20 has been made on a lifting entry vehicle with a hypersonic lift-drag ratio of about 3. The results indicate that although normal force can be predicted rather well, the lift-drag ratio is overpredicted by as much as 0.7. The experimental center of pressure was consistently forward of the theoretical location although the forward

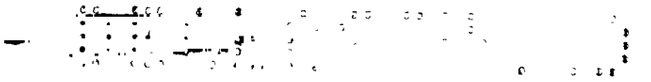

movement with increasing Mach number was adequately predicted. Directional and lateral stability parameters could not be calculated reliably.

Experimental results at a Mach number of 10 indicate that the basic body shape has a maximum untrimmed lift-drag ratio of about 3.2 but is longitudinally and directionally unstable throughout the test angle-of-attack range and has a region of lateral instability at the lower angles of attack. Addition of an undeflected elevon and a tip fin rolled out 20° and toed in 5° resulted in a configuration which trims at a lift-drag ratio of about 2.9 and is directionally and laterally stable above an angle of attack of about 4°. By use of aft body modifications in place of discrete tip fins, the vehicle trimmed at a lift-drag ratio of 2.8, was directionally stable at positive angles of attack, but was laterally unstable below the angle of attack for maximum lift-drag ratio.

Langley Research Center,
National Aeronautics and Space Administration,
Langley Station, Hampton, Va., February 2, 1970.

REFERENCES

1. Love, Eugene S.: Earth Orbital Logistics Spacecraft: Performance Aspects and Vehicle Concepts. Paper presented at the 1968 SAE Space Technology Conference (Washington, D.C.), May 1968.

2. Coward, Ken S.; Brevig, Ola; Ravenscroft, W.; and Ring, R.: Analytical Studies of the Use of the Propulsive-Lift Concept for the Descent and Landing of Manned Entry Vehicles (PLAME). NASA CR-66171, 1967.

3. Emigh, H. E.: Studies for the Use of Deployable Rotors for Final Descent and Landing of Reentry Vehicles. NASA CR-66707.

4. Schaefer, William T., Jr.: Characteristics of Major Active Wind Tunnels at the Langley Research Center. NASA TM X-1130, 1965.

TABLE I.- TEST PARAMETERS

Facility	Model length, l		Dynamic pressure, q		Mach number, M	Reynolds number, R
	in.	cm	lb/ft^2	kN/m^2		
Langley 20-inch hypersonic tunnel (Mach 6)	12.6	32.0	188	9.00	5.9	1.6×10^6
	12.6	32.0	504	24.13	6.0	4.5
	12.6	32.0	720	34.47	6.0	6.9
	12.6	32.0	1058	50.66	6.0	8.9
Langley continuous-flow hypersonic tunnel	12.6	32.0	150	7.18	10.3	1.0×10^6
	12.6	32.0	241	11.54	10.3	1.6
	12.6	32.0	331	15.85	10.4	2.1
	31.5	80.0	241	11.54	10.3	4.7
Langley 22-inch helium tunnel	12.6	32.0	92	4.40	18.1	1.7×10^6
	12.6	32.0	134	6.42	19.0	4.5
	12.6	32.0	230	11.01	20.0	6.9
	12.6	32.0	365	17.48	21.6	8.9

TABLE II.- BALANCE ACCURACY

M	R	C_N	C_A	C_m	C_l	C_n	C_Y
5.9	1.6×10^6	0.0031	0.0005	0.0002	0.0005	0.0008	0.0018
6.0	4.5	.0011	.0002	.0001	.0002	.0003	.0007
6.0	6.9	.0008	.0001	.0001	.0001	.0002	.0005
6.0	8.9	.0005	.0001	.0000	.0001	.0001	.0003
10.3	1.0	.0029	.0010	.0002	.0006	.0005	.0015
10.3	1.6	.0017	.0006	.0002	.0004	.0003	.0010
10.4	2.1	.0013	.0004	.0001	.0003	.0002	.0007
10.3	4.7	.0031	.0006	.0001	.0001	.0001	.0011
18.1	1.7	.0038	.0013	.0002	.0004	.0004	.0013
19.0	4.5	.0026	.0009	.0001	.0003	.0003	.0009
20.0	6.9	.0015	.0005	.0001	.0001	.0001	.0005
21.6	8.9	.0009	.0003	.0001	.0001	.0001	.0003

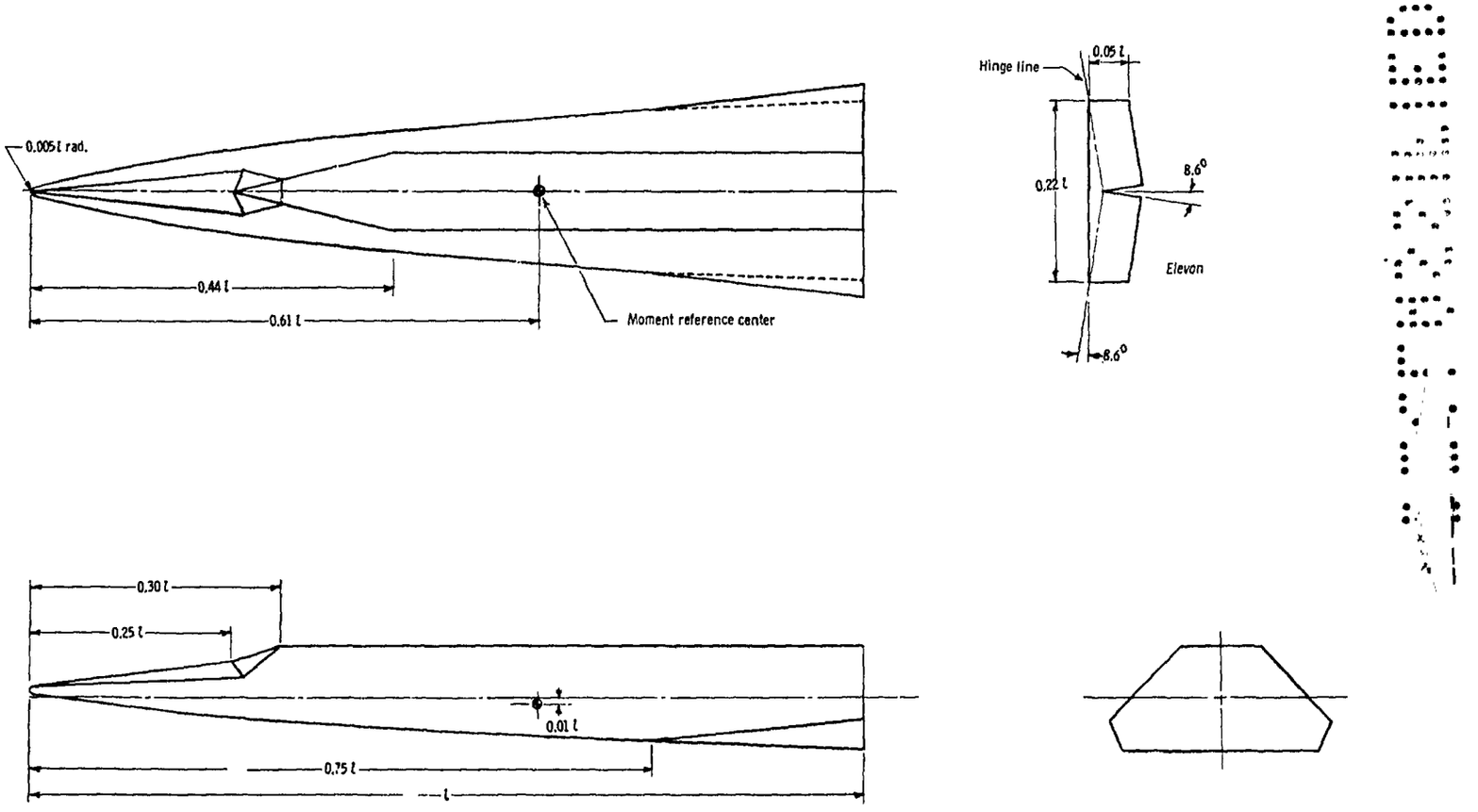

Figure 1.- Basic body (DL-4A) and elevon details. All dimensions are given in percent of actual body length.

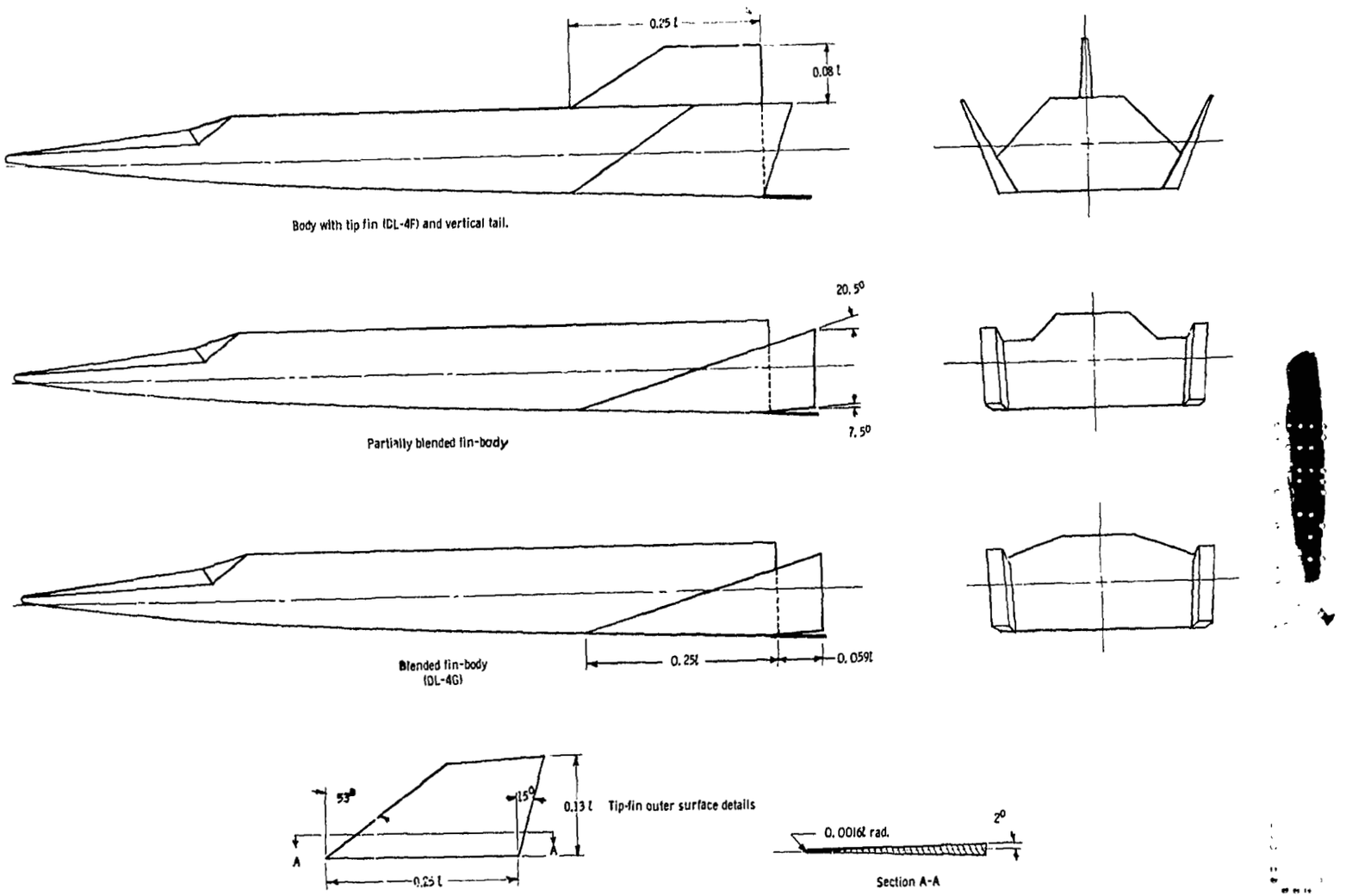

Figure 2.- Fins and aft body modifications.

(a) Small basic body and large body with tip-fins.

L-68-10 322.1

Figure 3.- Model photographs.

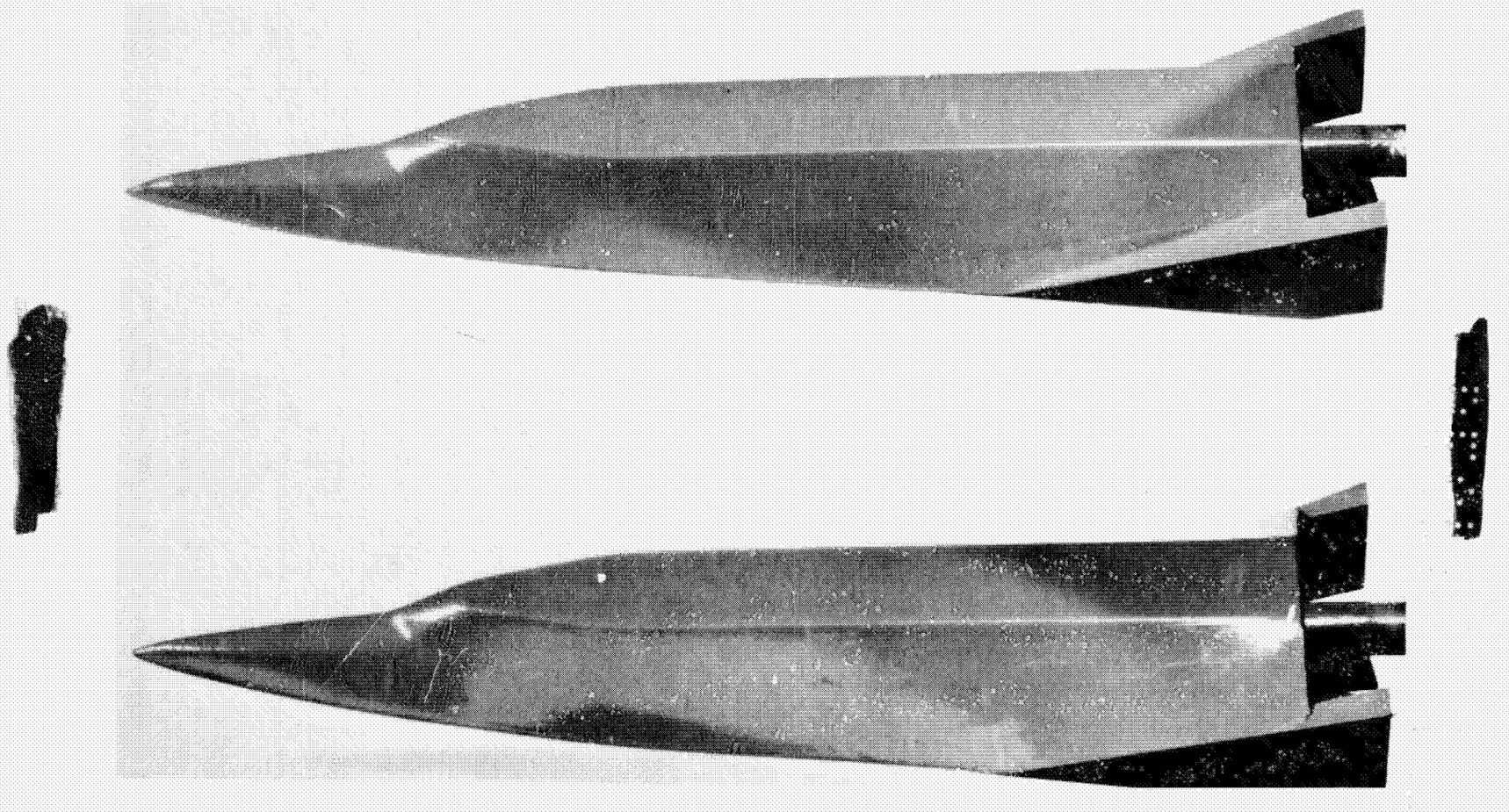

(b) Partially blended and fully blended bodies. L-69-2415

Figure 3.- Concluded.

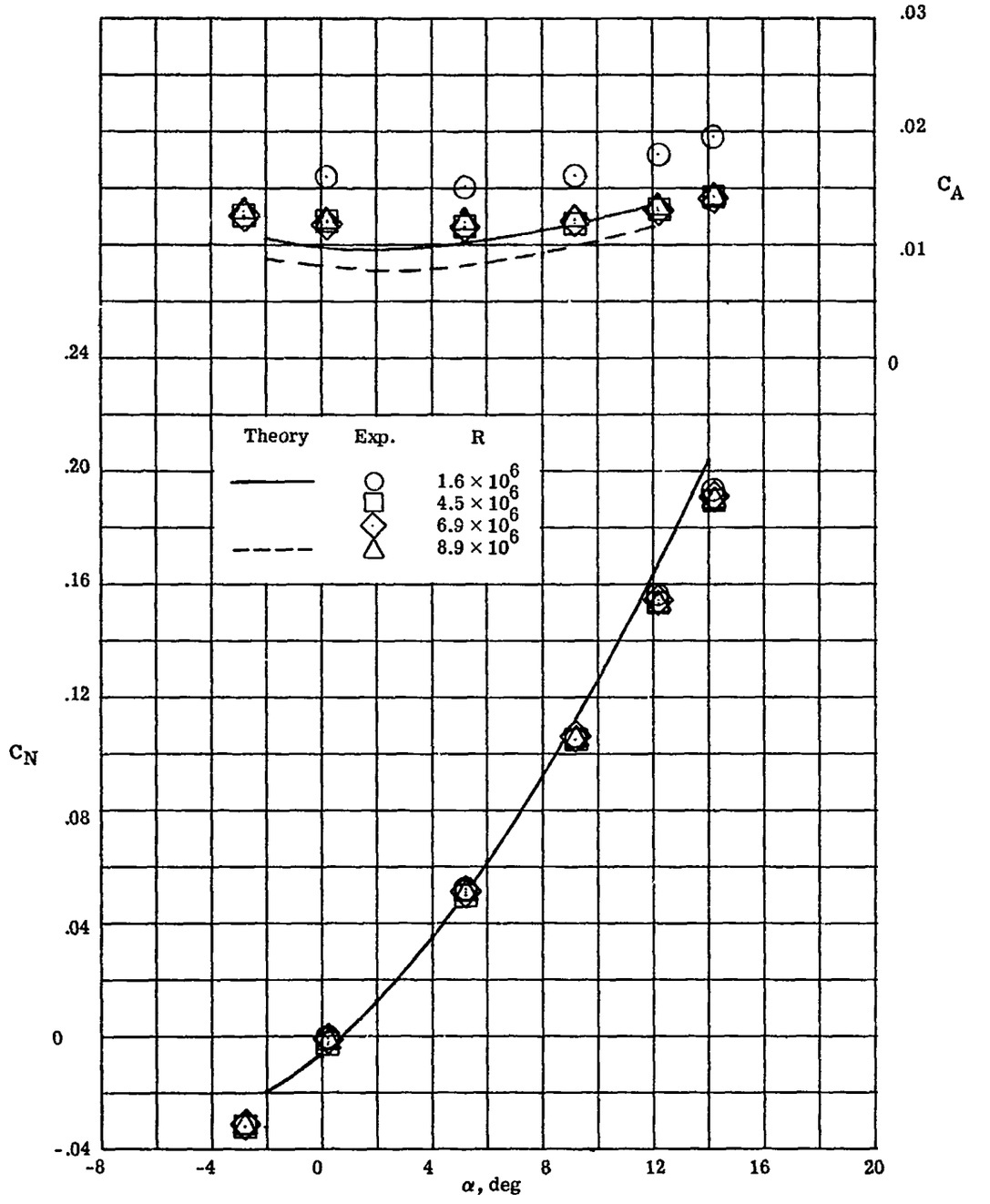

(a) M = 6.0 in air.

Figure 4.- Comparison of theoretical and experimental normal- and axial-force coefficients of basic body (DL-4A) for several Reynolds numbers.

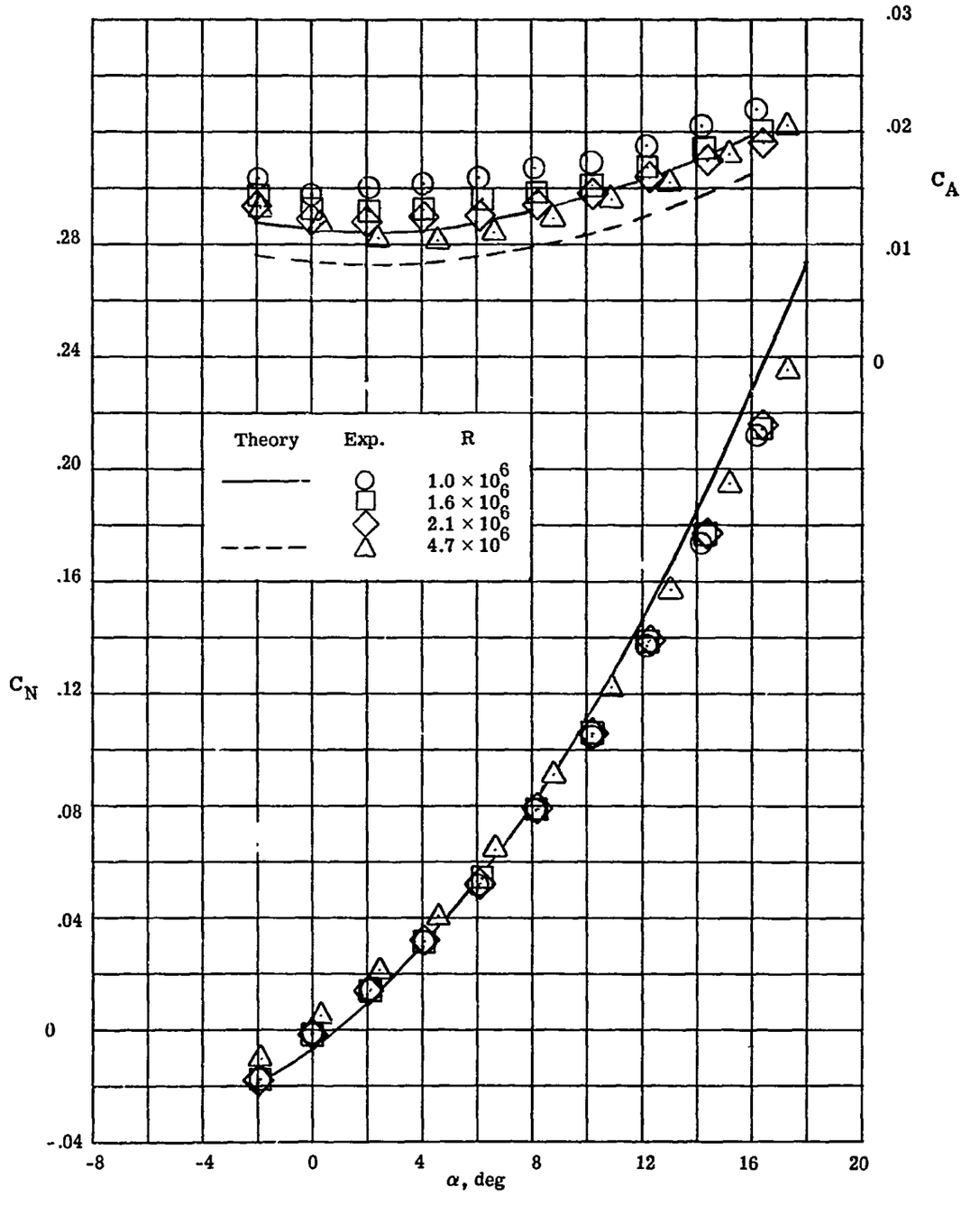

(b) M = 10.3 in air.

Figure 4.- Continued.

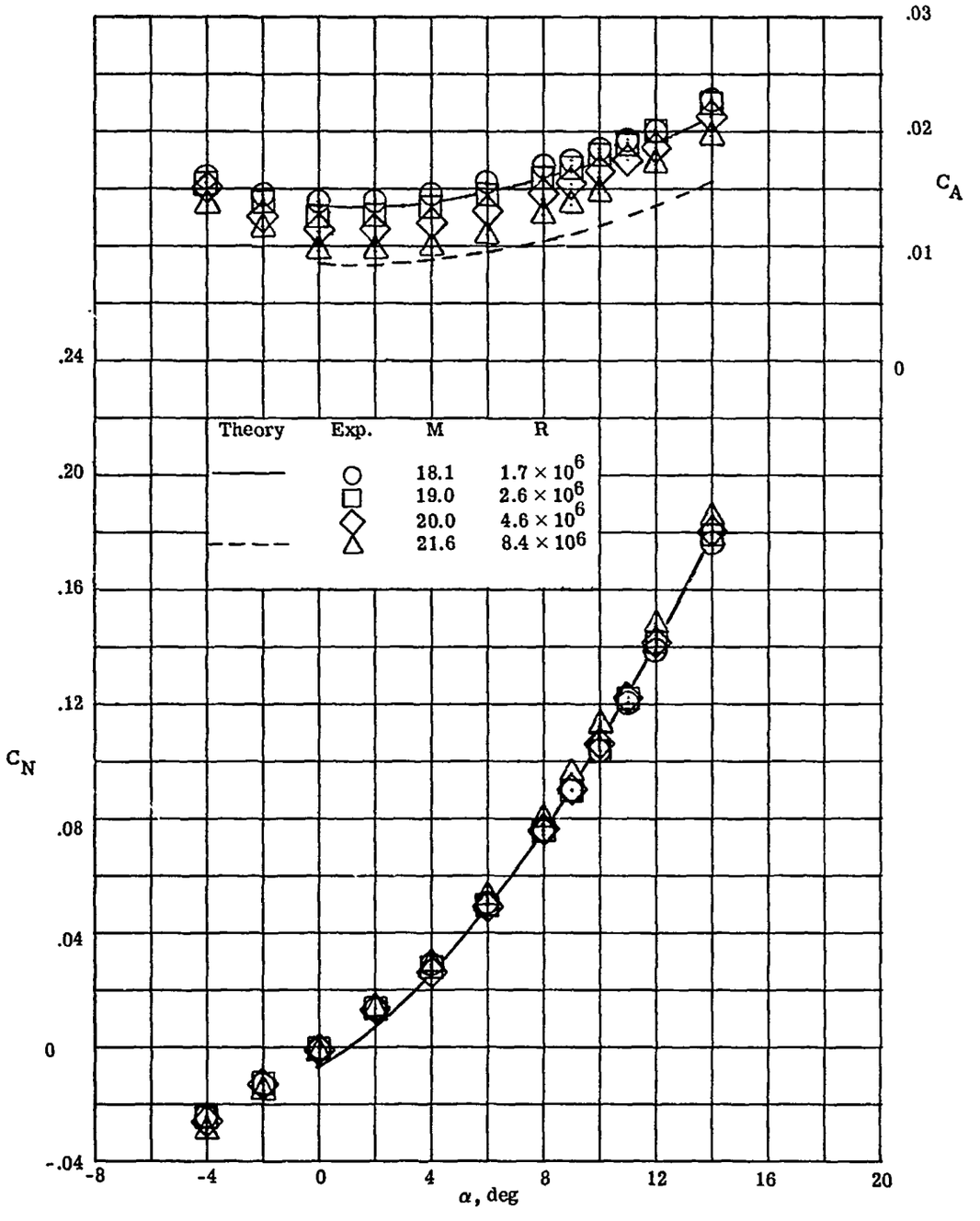

(c) $M \approx 20$ in helium.

Figure 4.- Concluded.

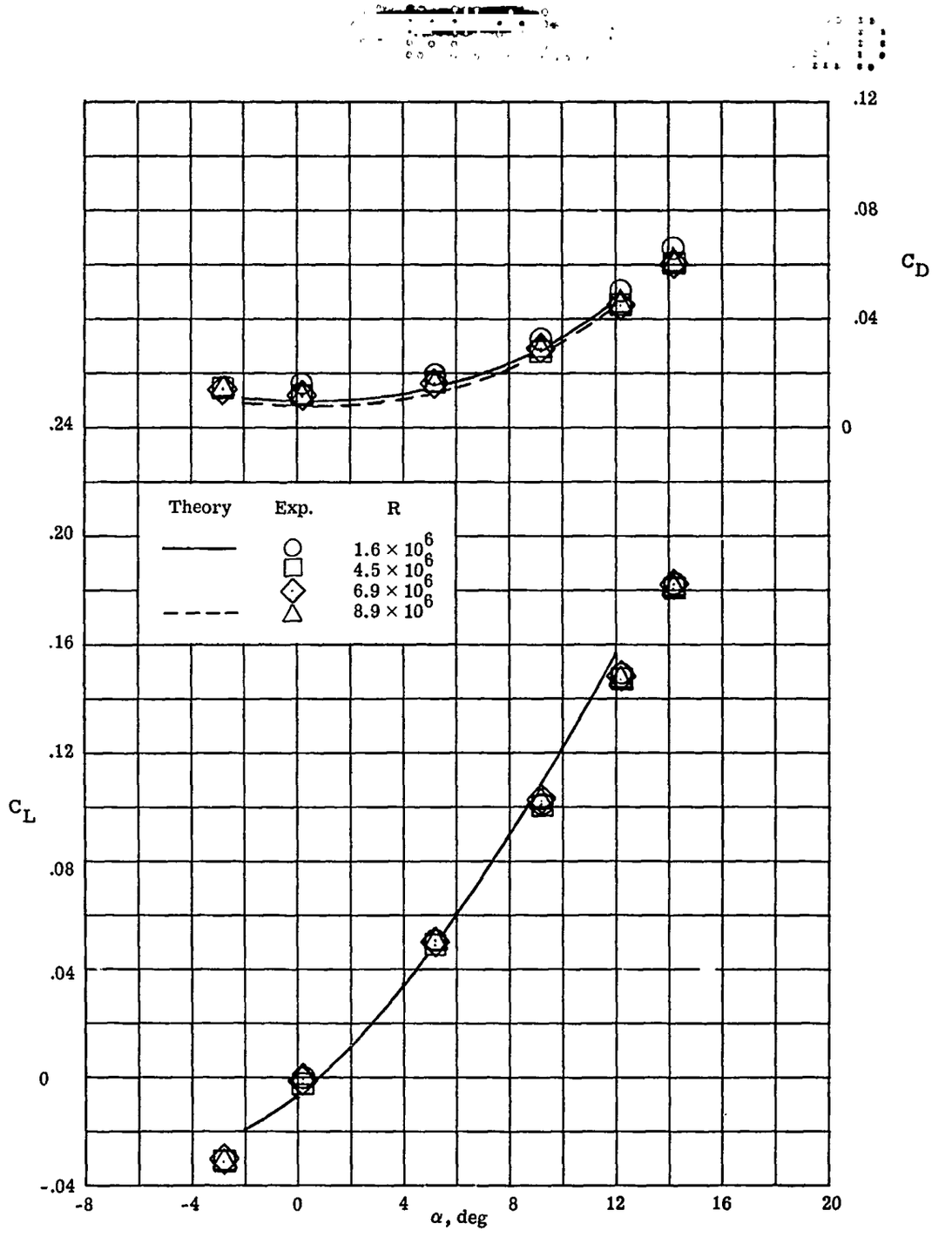

(a) M = 6.0 in air.

Figure 5.- Comparison of theoretical and experimental lift and drag coefficients of basic body (DL-4A) for several Reynolds numbers.

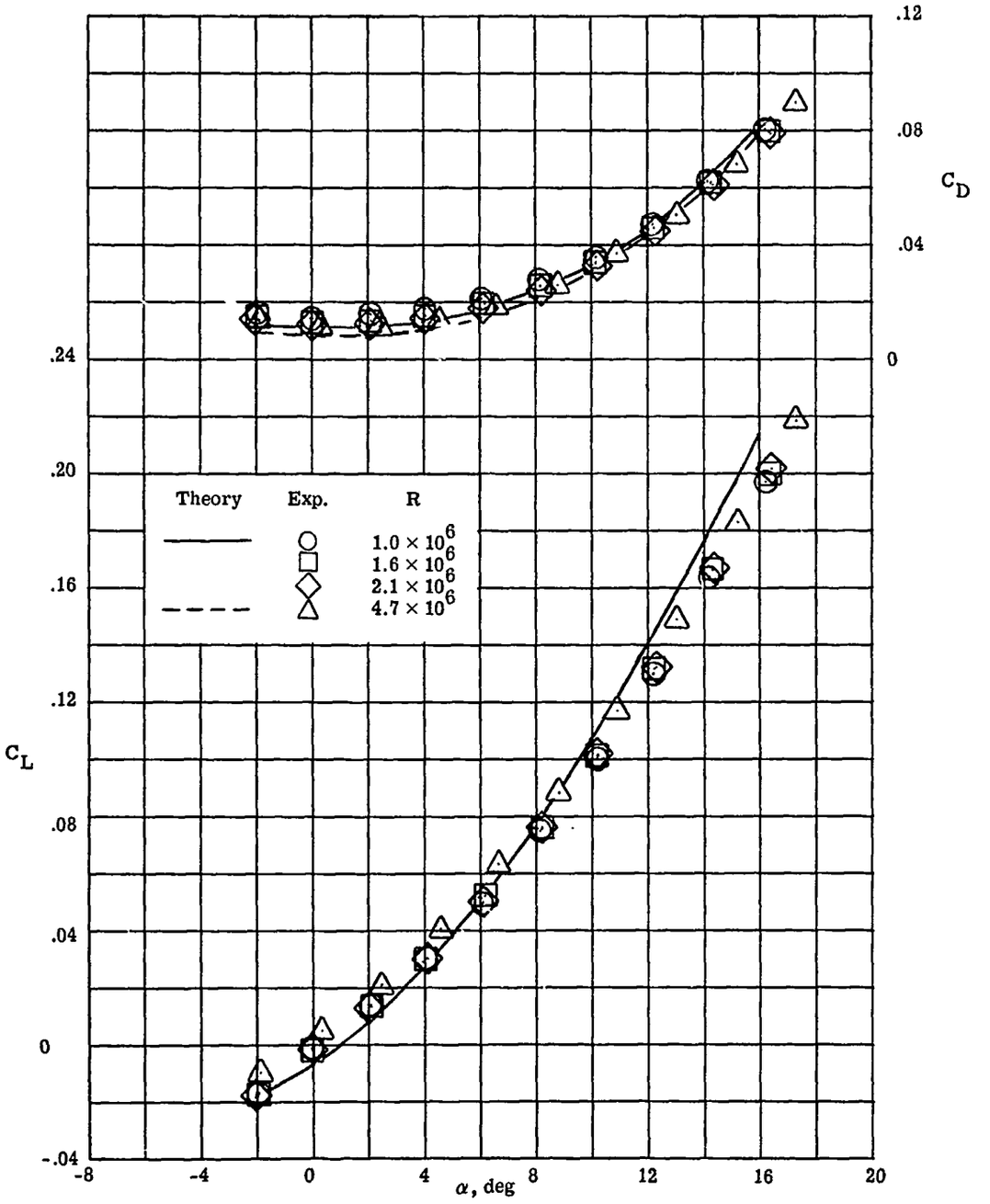

(b) M = 10.3 in air.

Figure 5.- Continued.

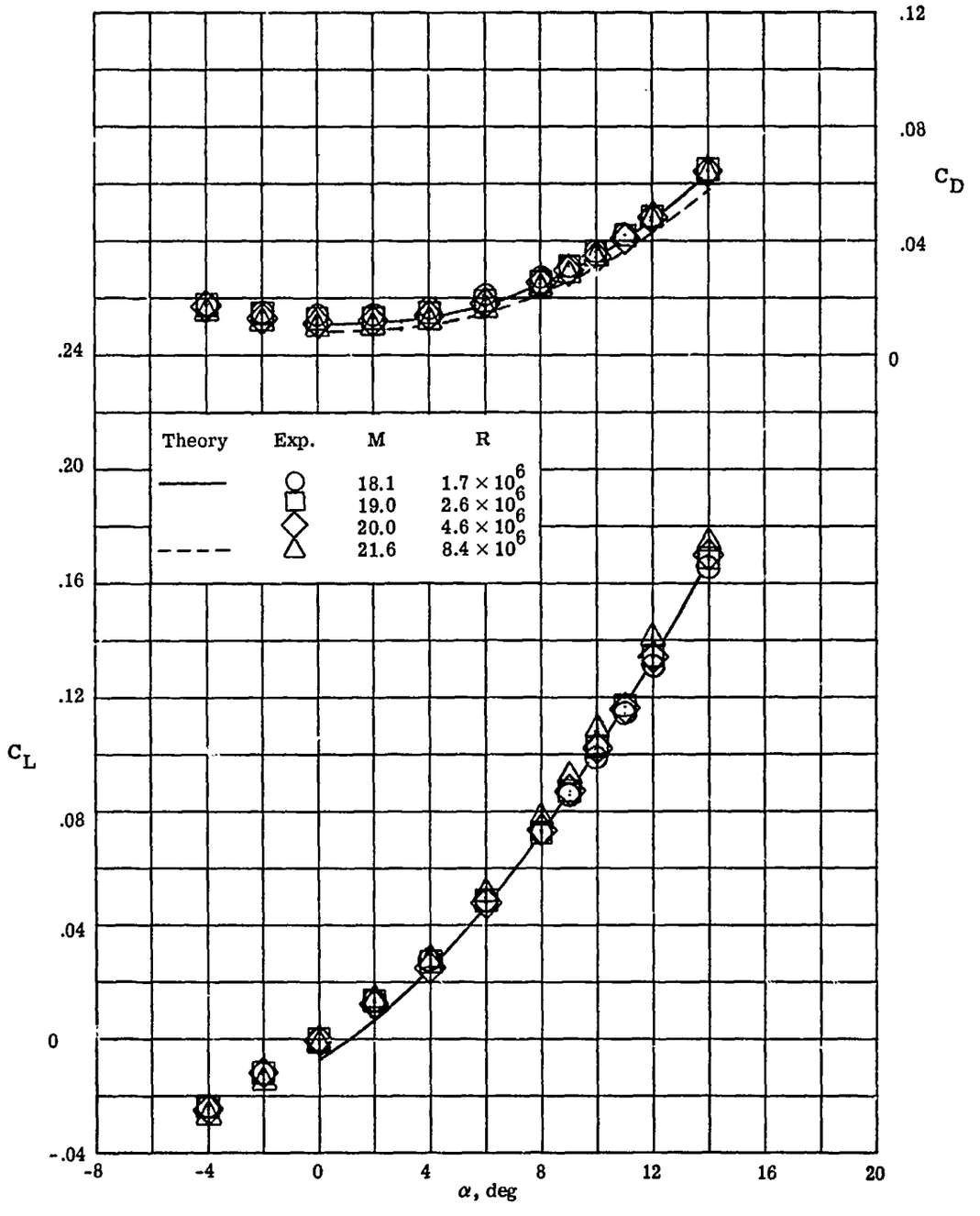

(c) $M \approx 20$ in helium.

Figure 5.- Concluded.

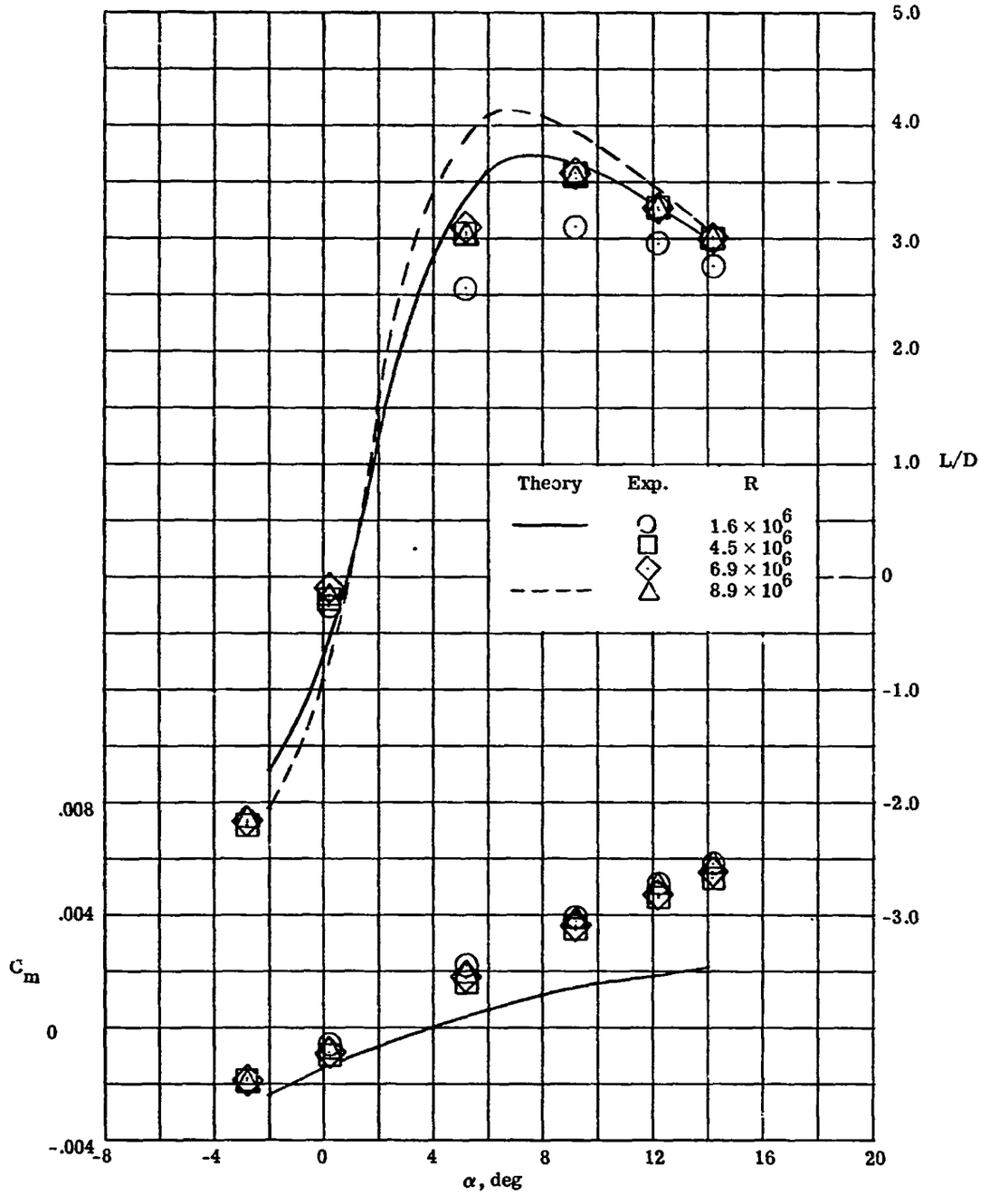

(a) M = 6.0 in air.

Figure 6.- Comparison of theoretical and experimental lift-drag ratios and pitching-moment coefficients of basic body (DL-4A) for several Reynolds numbers.

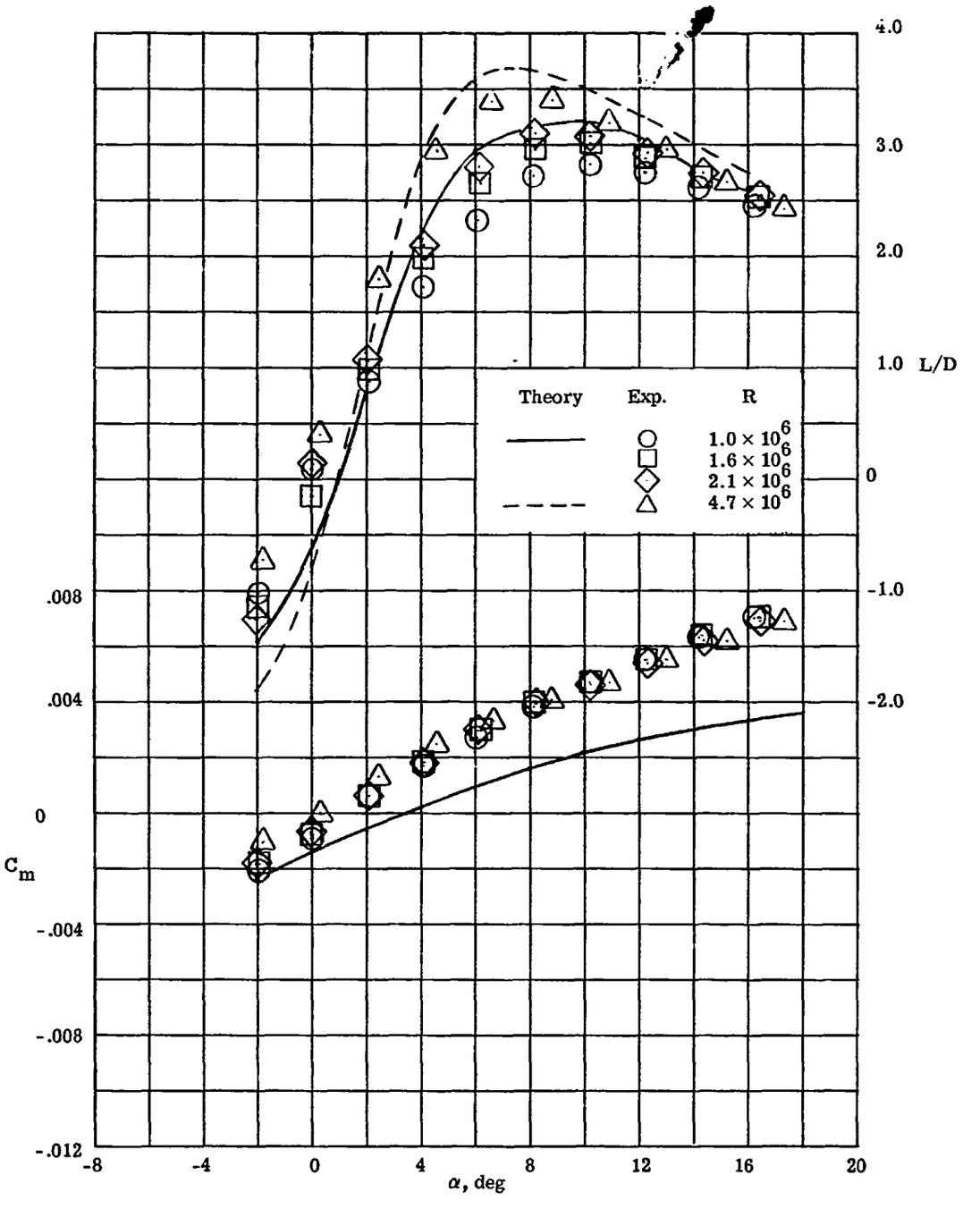

(b) M = 10.3 in air.

Figure 6.- Continued.

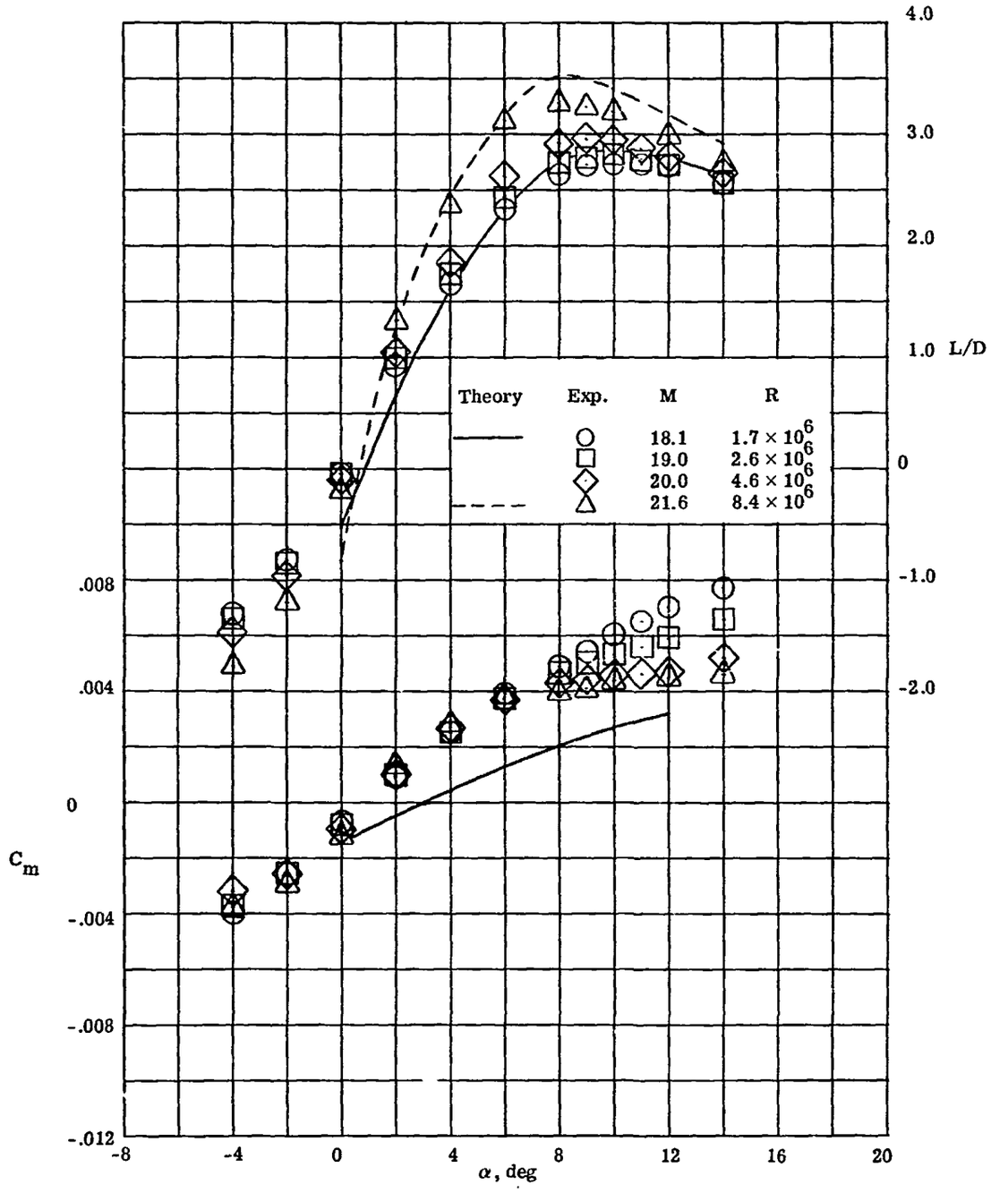

(c) $M \approx 20$ in helium.

Figure 6.- Concluded.

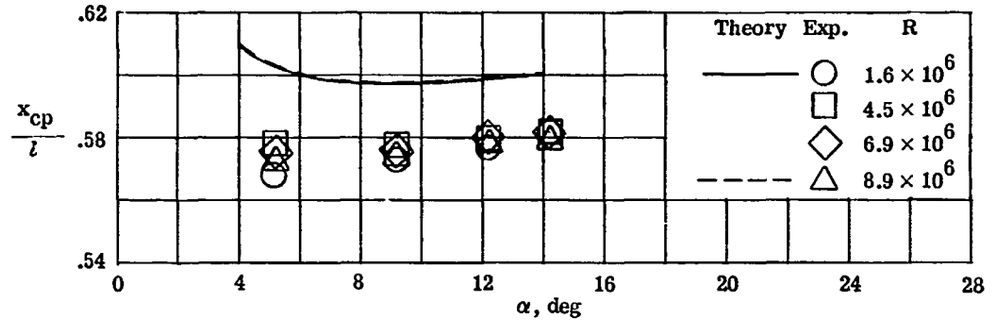

(a) M = 6.0 in air.

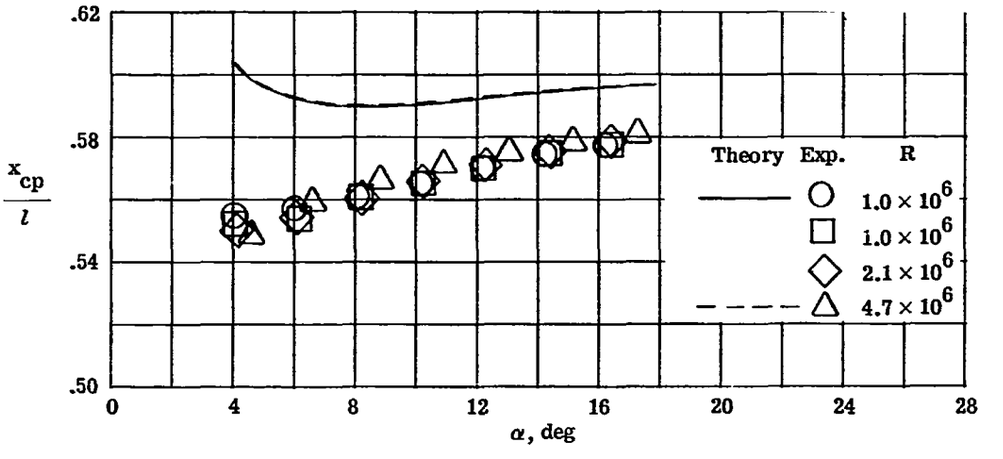

(b) M = 10.3 in air.

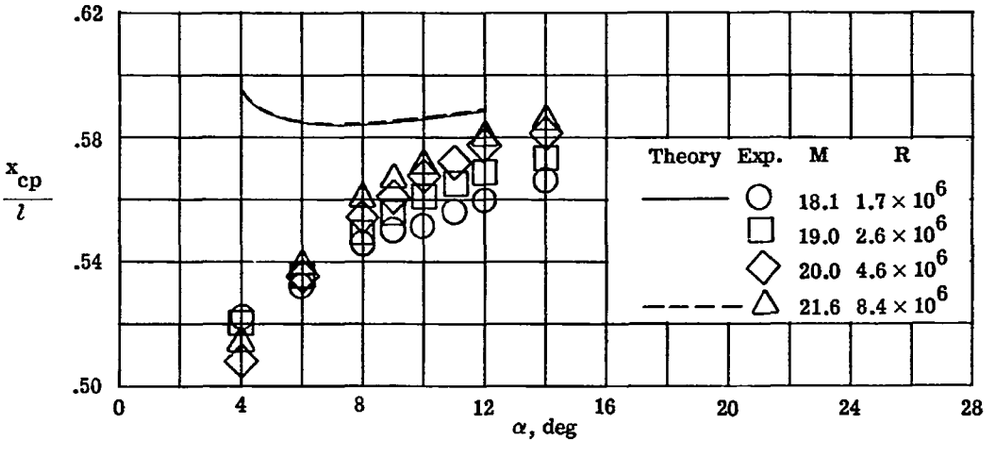

(c) M ≈ 20 in helium.

Figure 7.- Comparison of theoretical and experimental centers of pressure of basic body (DL-4A) for several Reynolds numbers.

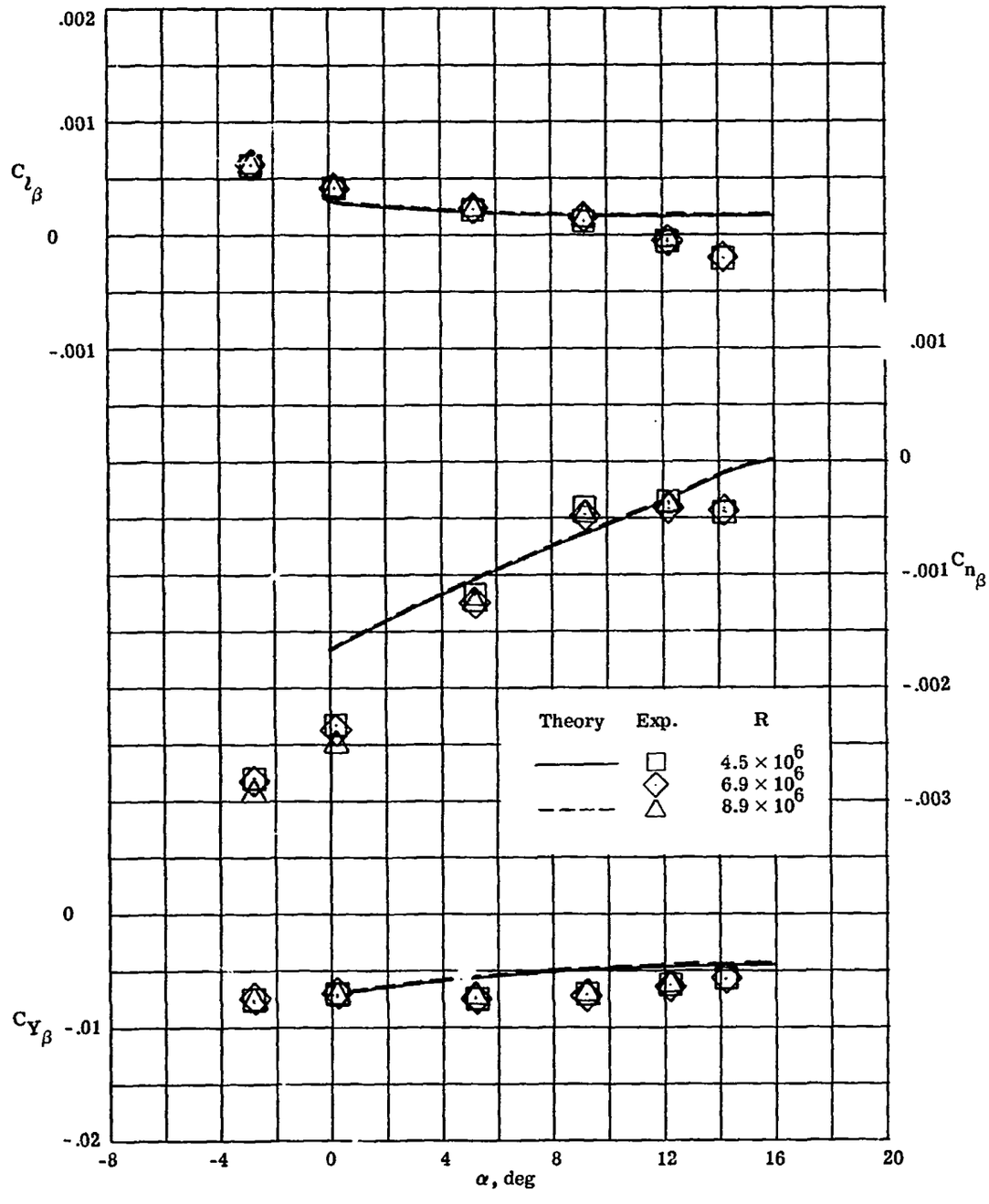

(a) M = 6.0 in air.

Figure 8.- Comparison of theoretical and experimental directional and lateral stability parameters of basic body (DL-4A) for several Reynolds numbers.

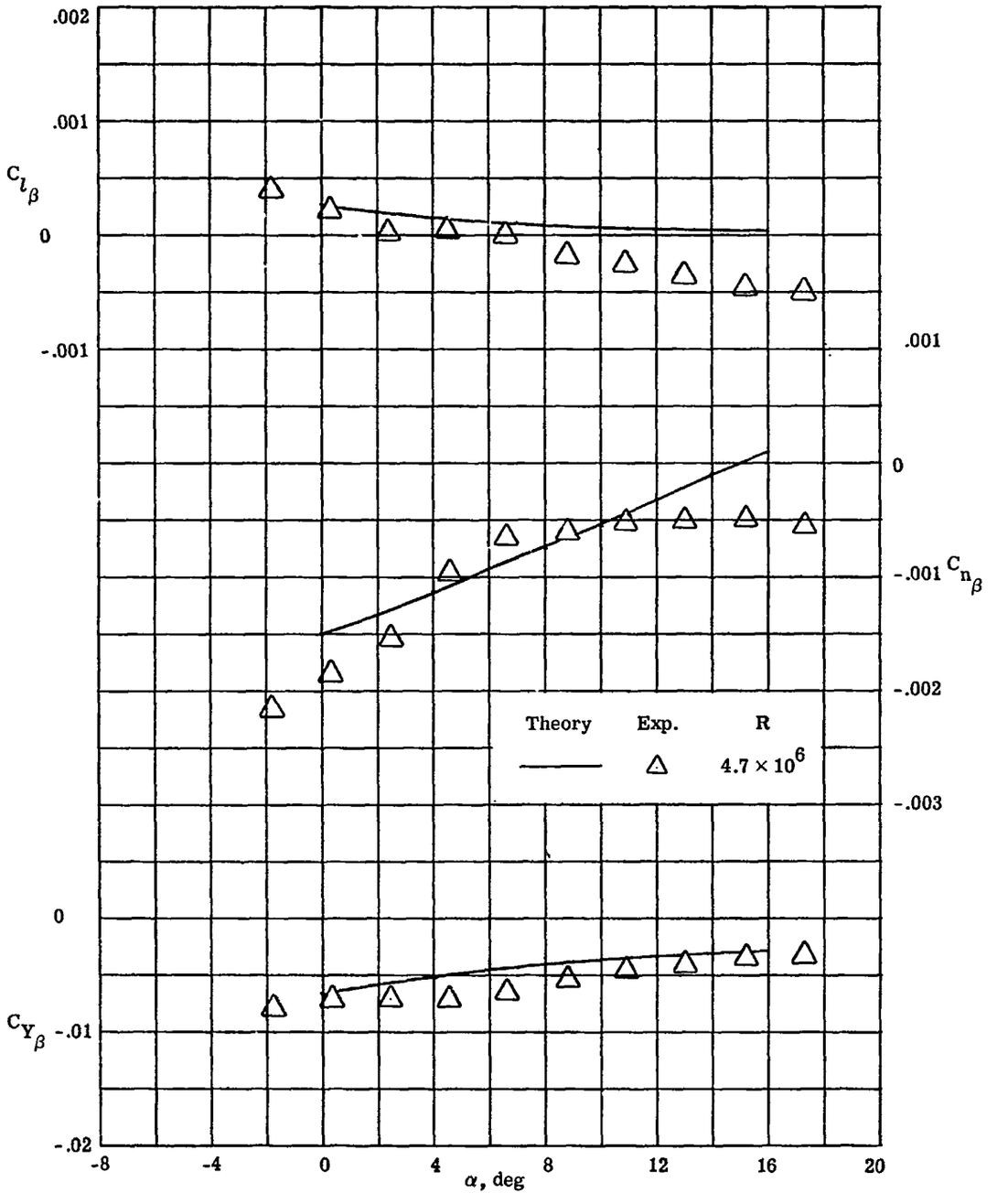

(b) M = 10.3 in air.

Figure 8.- Continued.

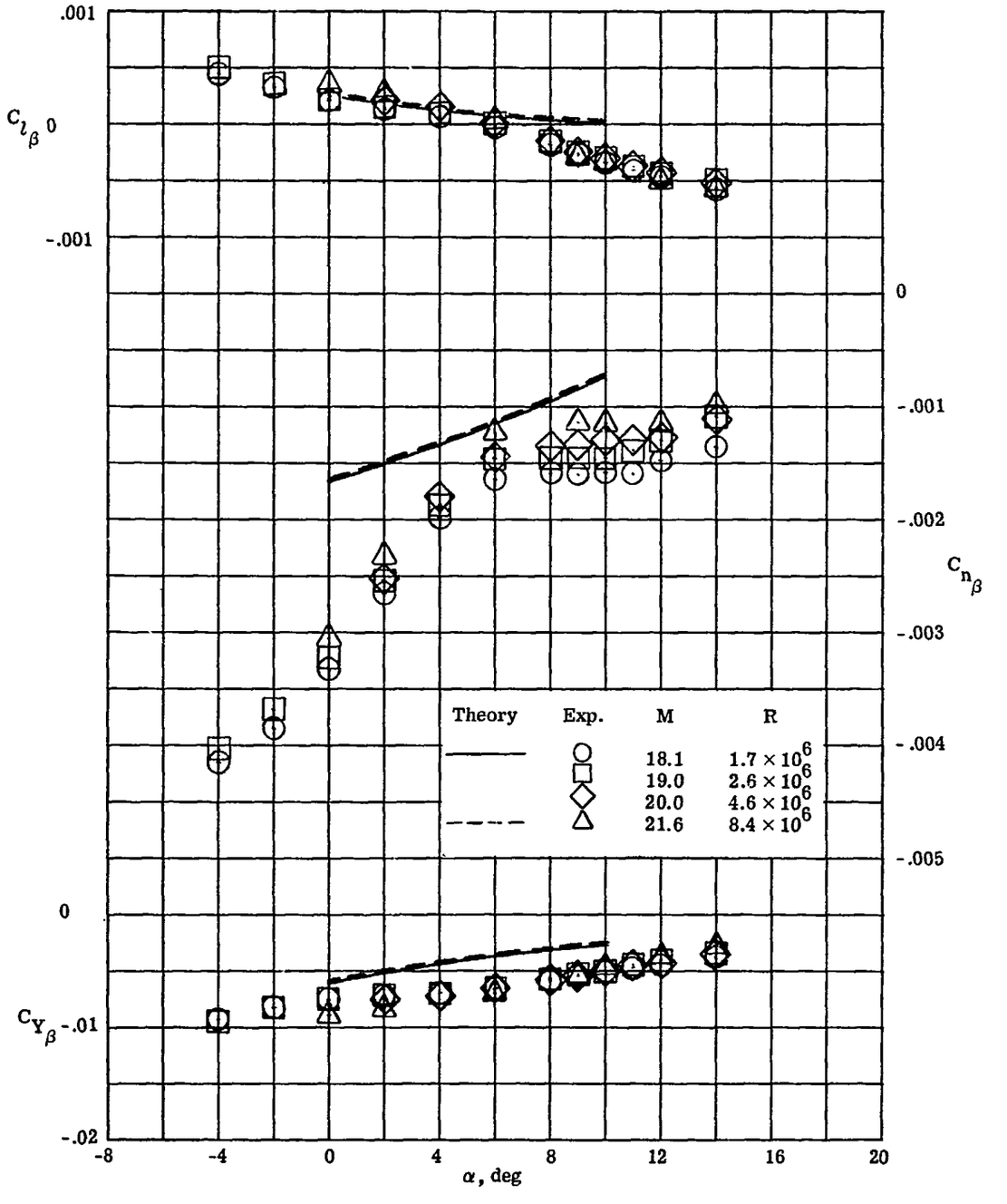

(c) M ≈ 20 in helium.

Figure 8.- Concluded.

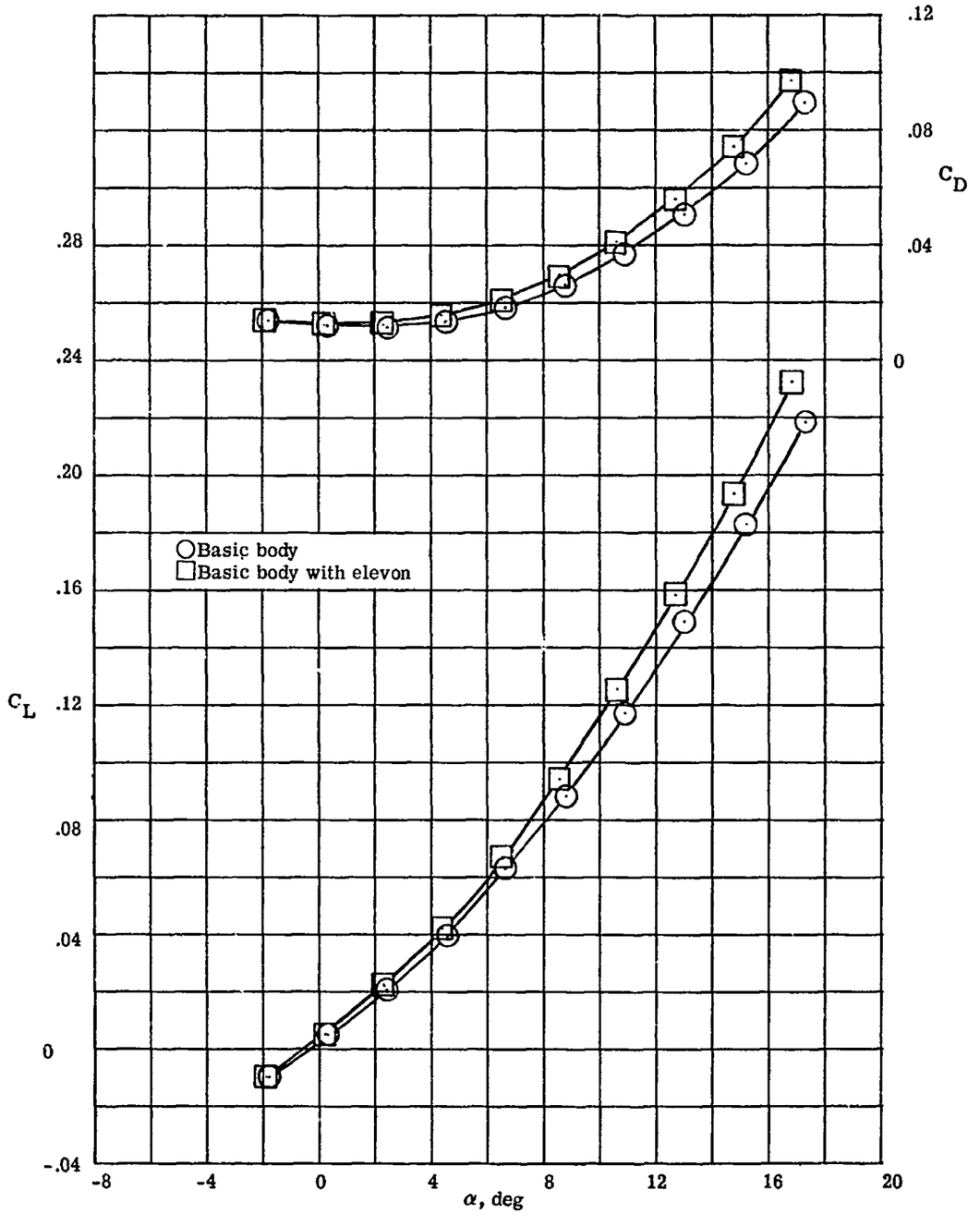

(a) Lift and drag coefficients.

Figure 9.- Effects of undeflected elevon on aerodynamic characteristics of basic body (DL-4A). M = 10.4; R = 4.7 × 10^6.

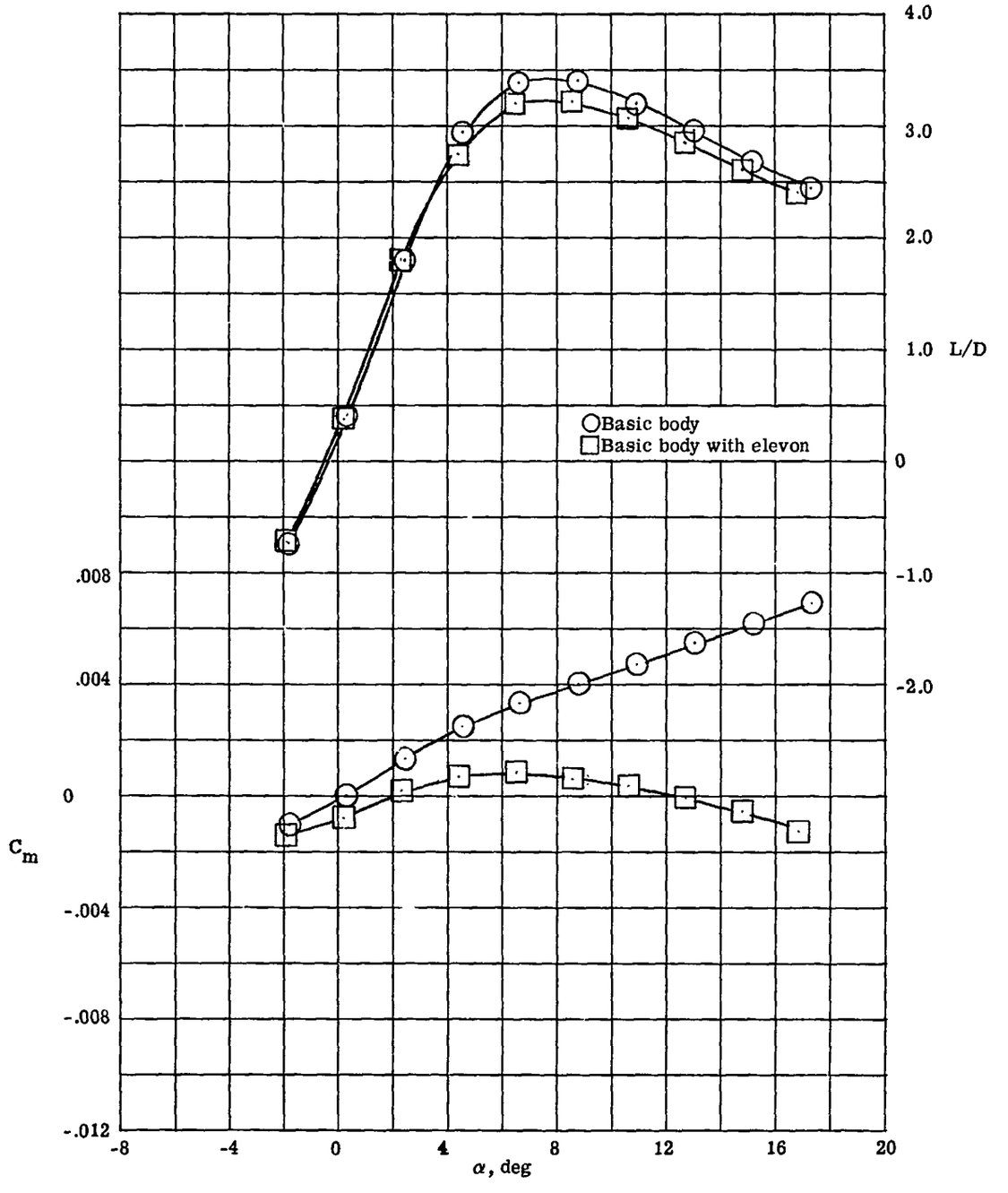

(b) Lift-drag ratio and pitching-moment coefficient.

Figure 9.- Continued.

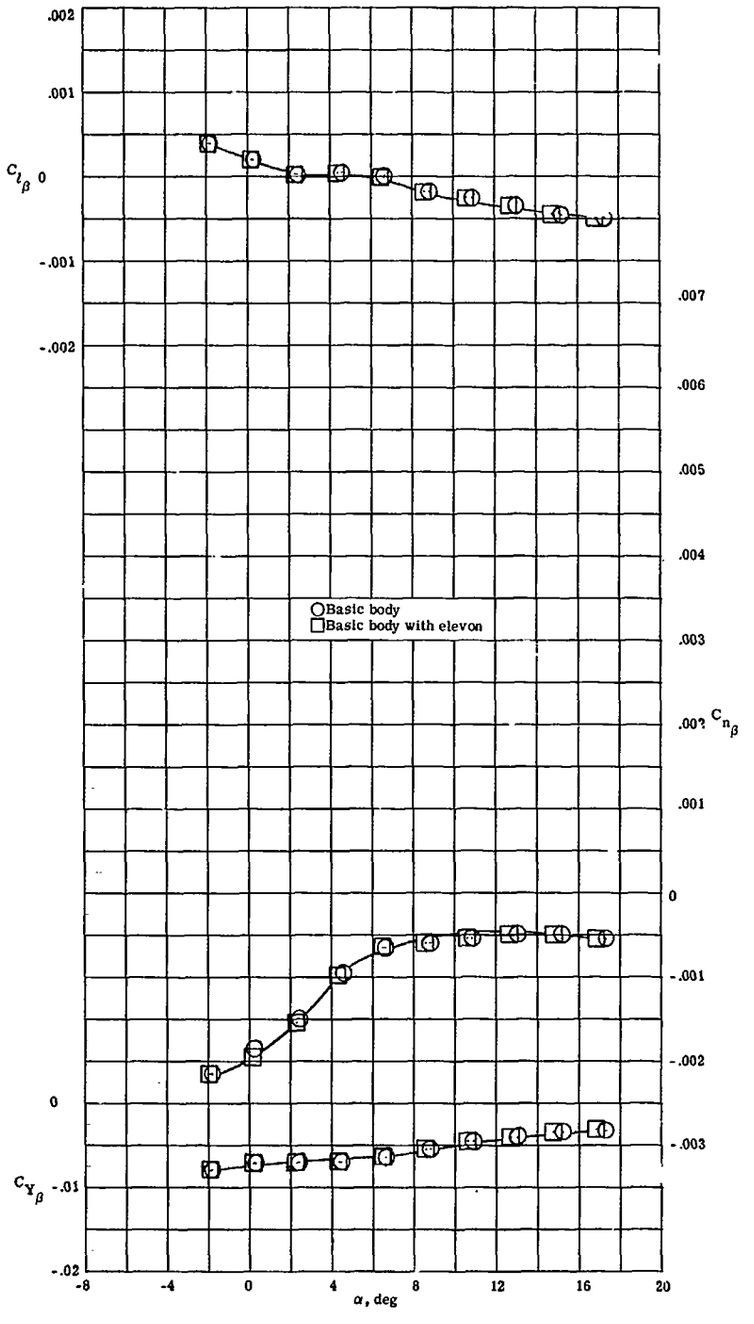

(c) Directional and lateral stability parameters.

Figure 9.- Concluded.

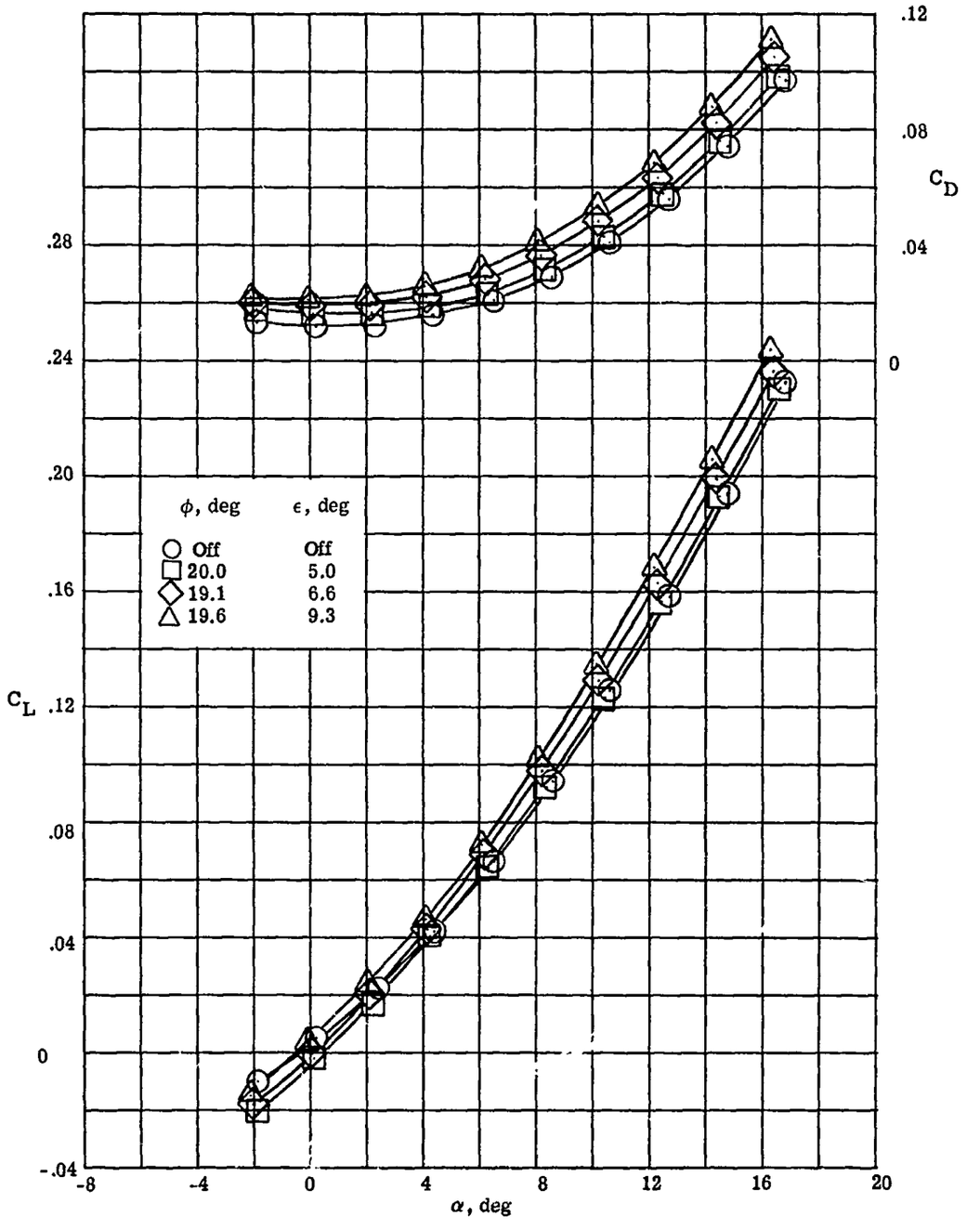

(a) Lift and drag coefficients.

Figure 10.- Effects of tip-fin toe-in angle on aerodynamic characteristics of configuration DL-4F. M = 10.4; R = 4.7 × 10^6.

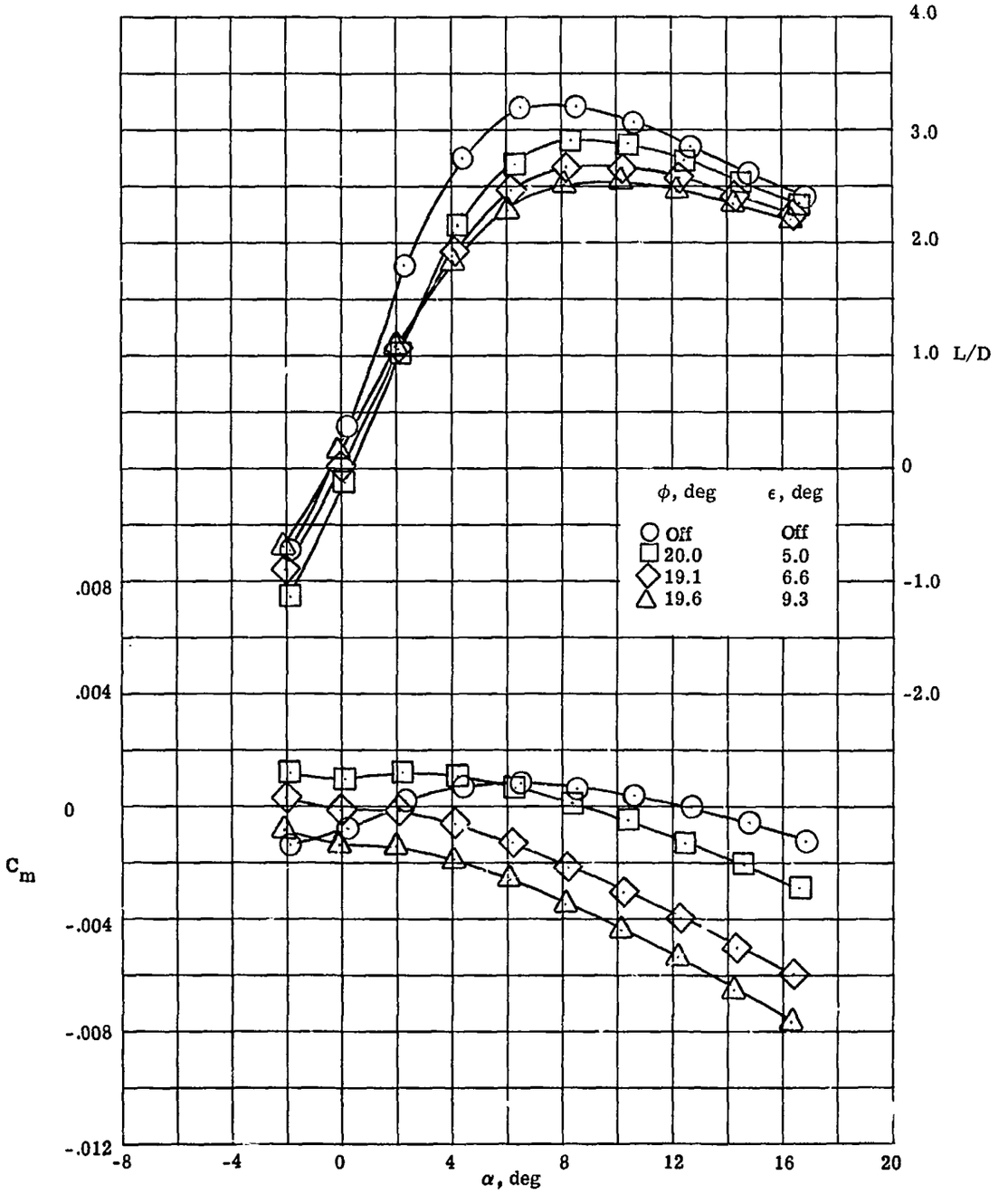

(b) Lift-drag ratio and pitching-moment coefficient.

Figure 10.- Continued.

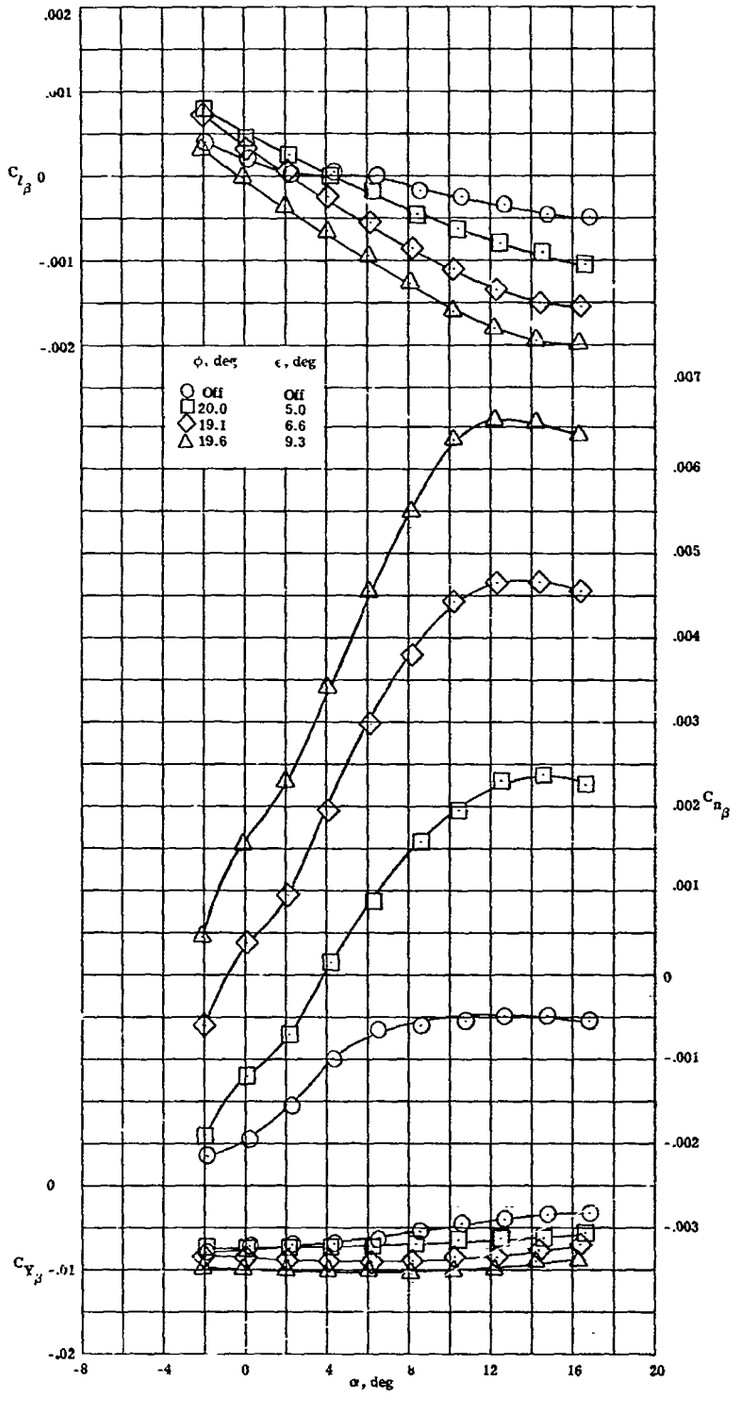

(c) Directional and lateral stability parameters.

Figure 10. Concluded.

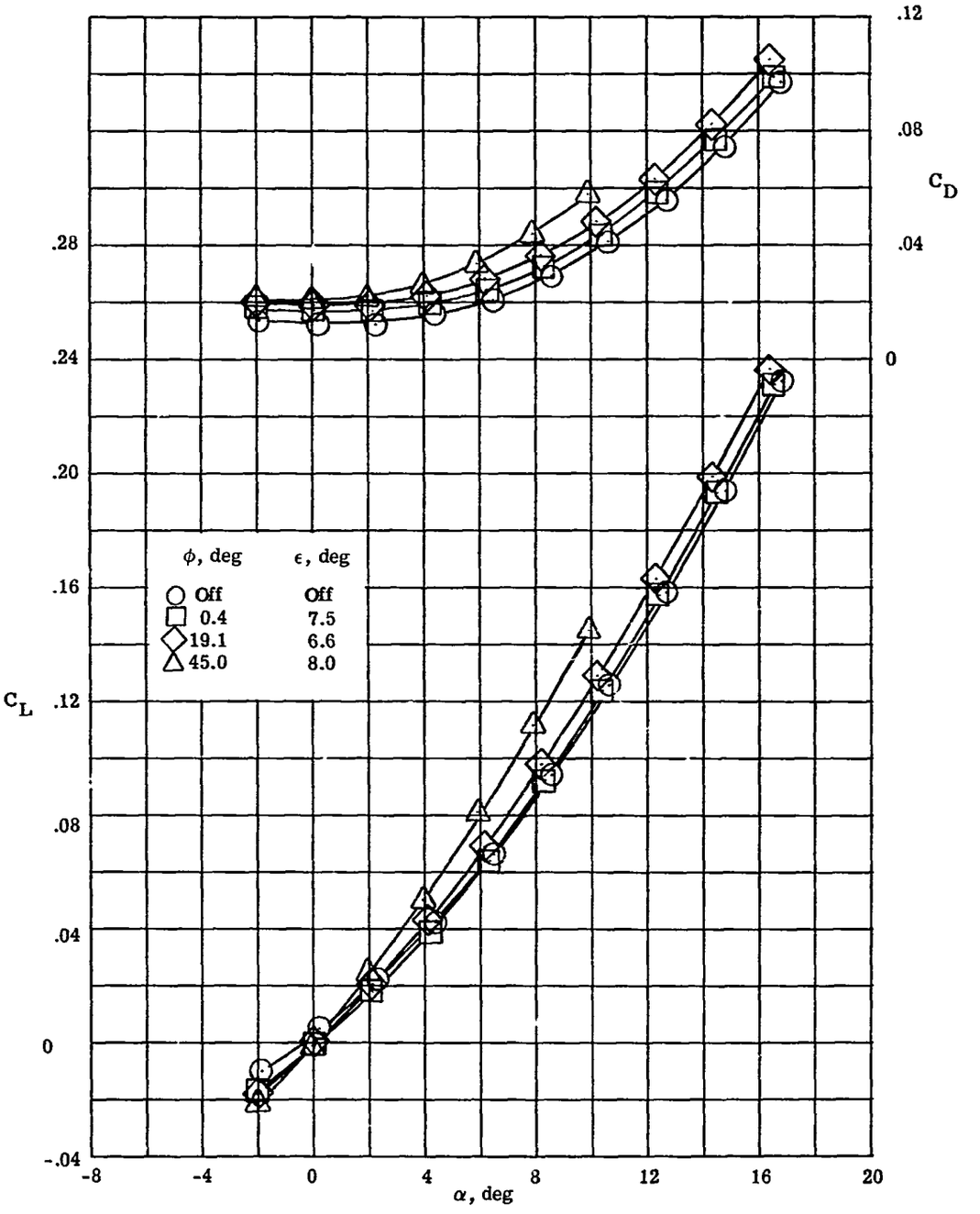

(a) Lift and drag coefficients.

Figure 11.- Effects of tip-fin roll-out angle on aerodynamic characteristics of configuration DL-4F. M = 10.4; R = 4.7 × 10^6.

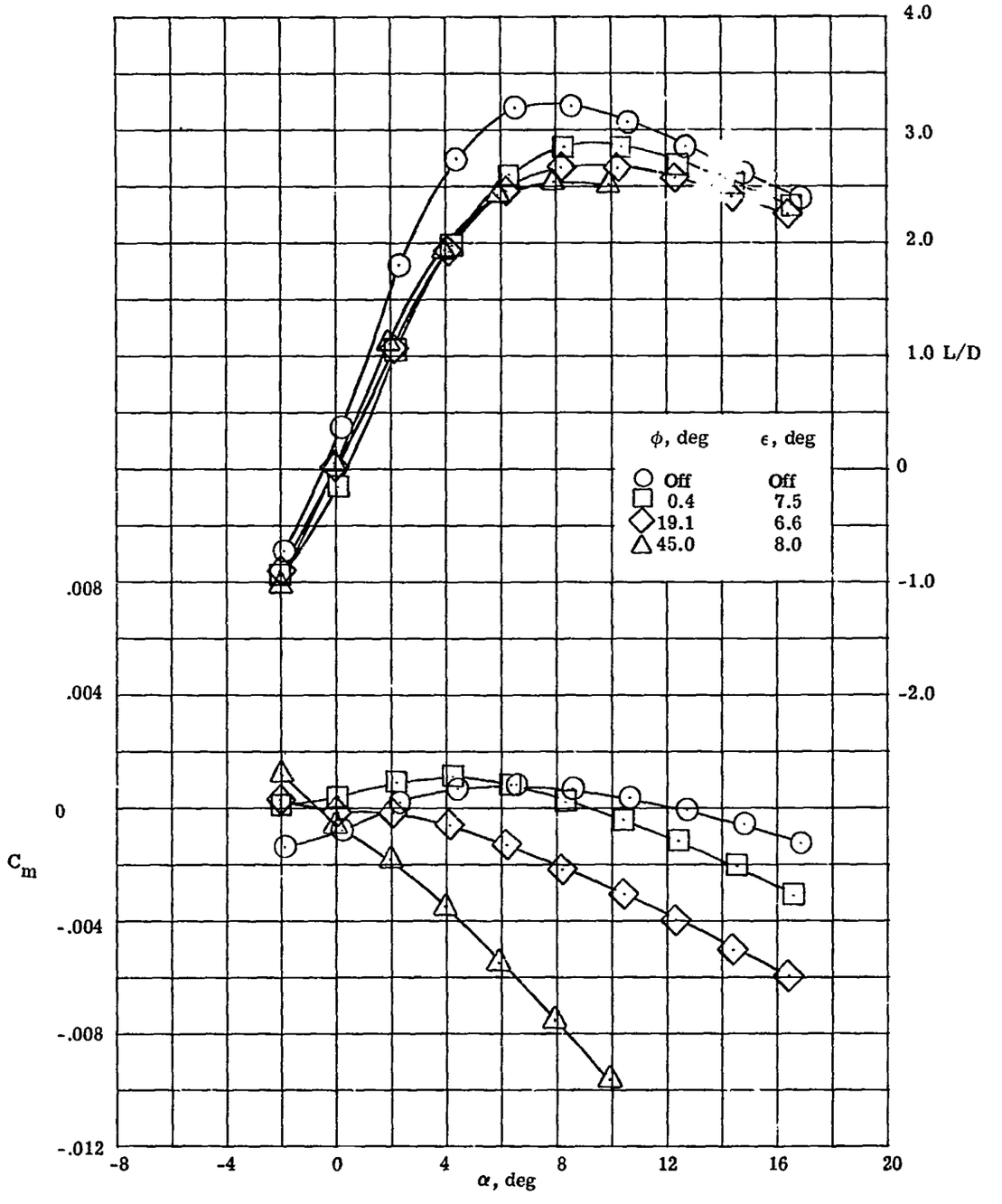

(b) Lift-drag ratio and pitching-moment coefficient.

Figure 11.- Continued.

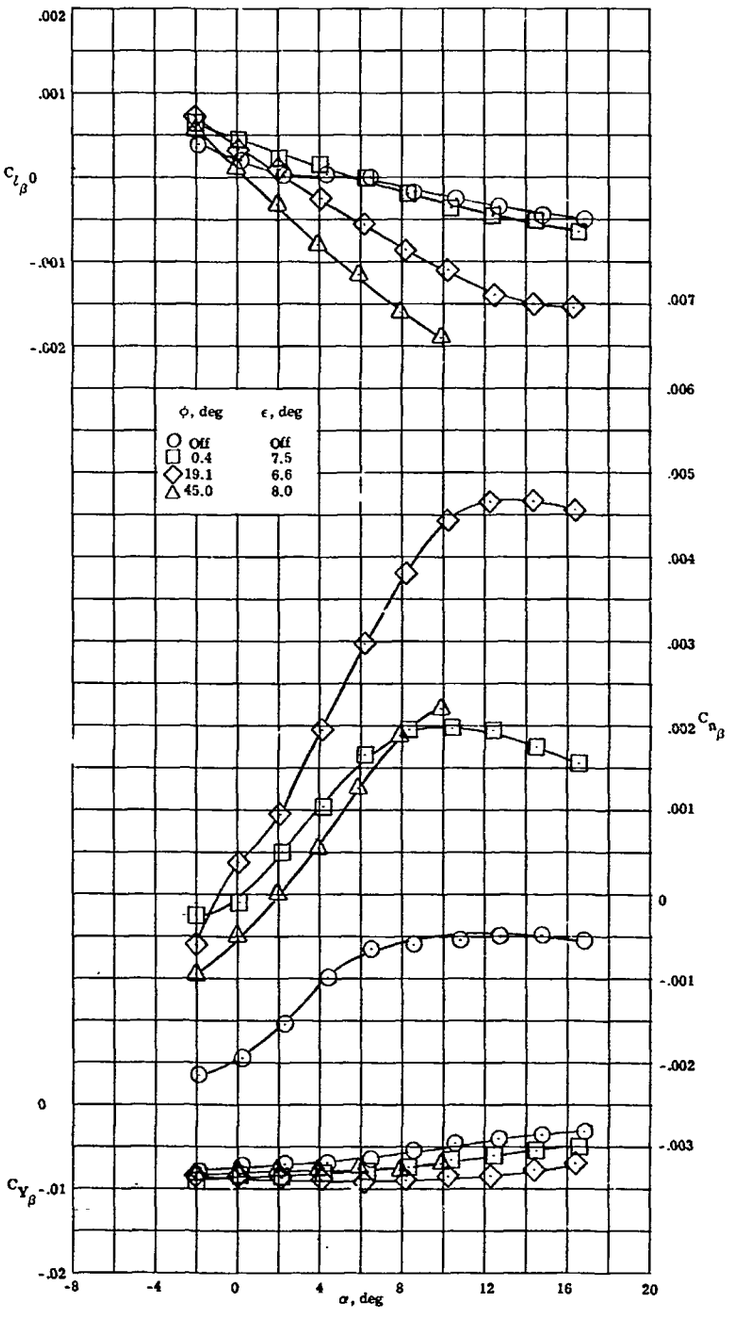

(c) Directional and lateral stability parameters.

Figure 11.- Concluded.

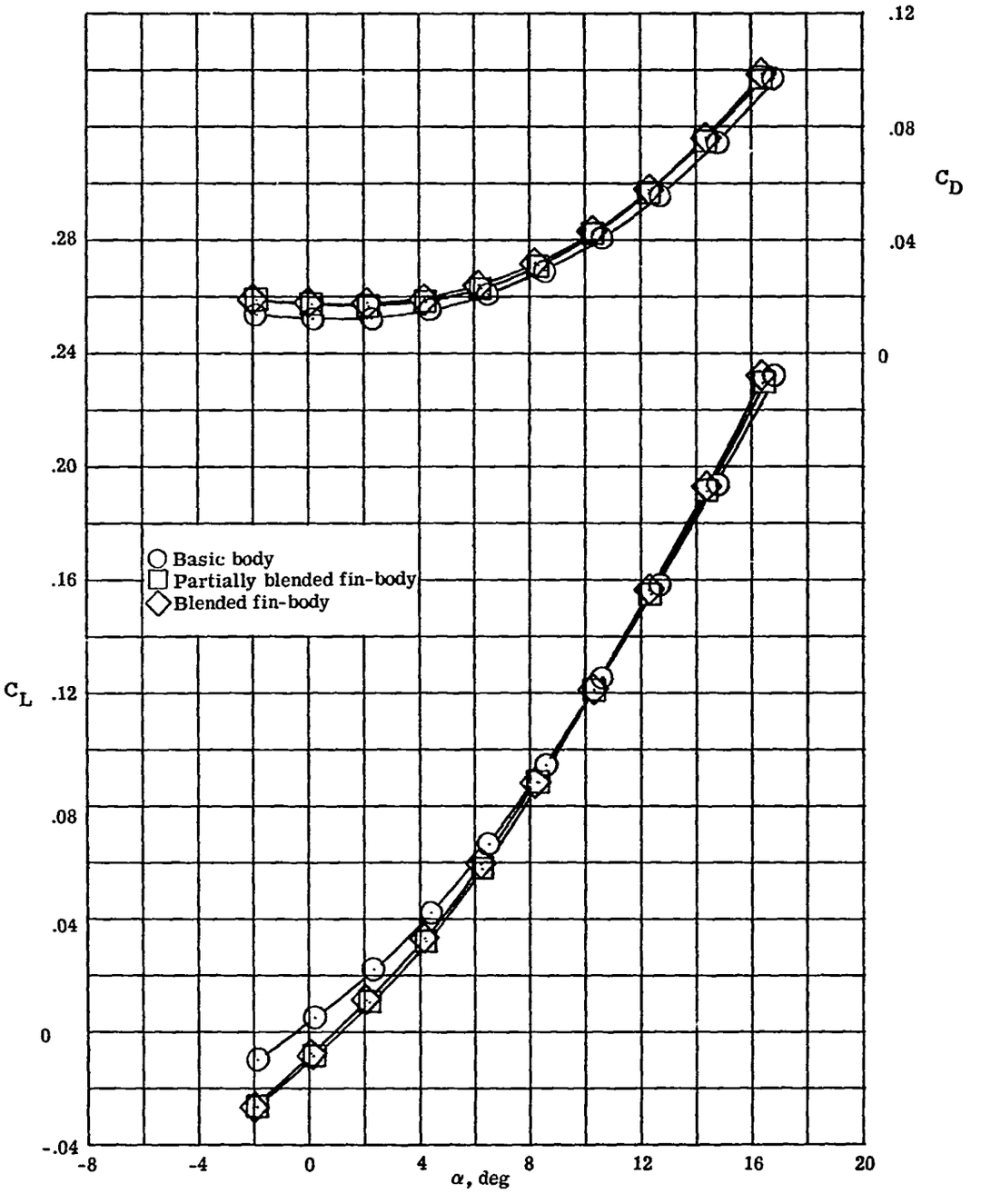

(a) Lift and drag coefficients.

Figure 12.- Effects of aft body modification on aerodynamic characteristics of configuration DL-4G. M = 10.4; R = 4.7 × 10^6,

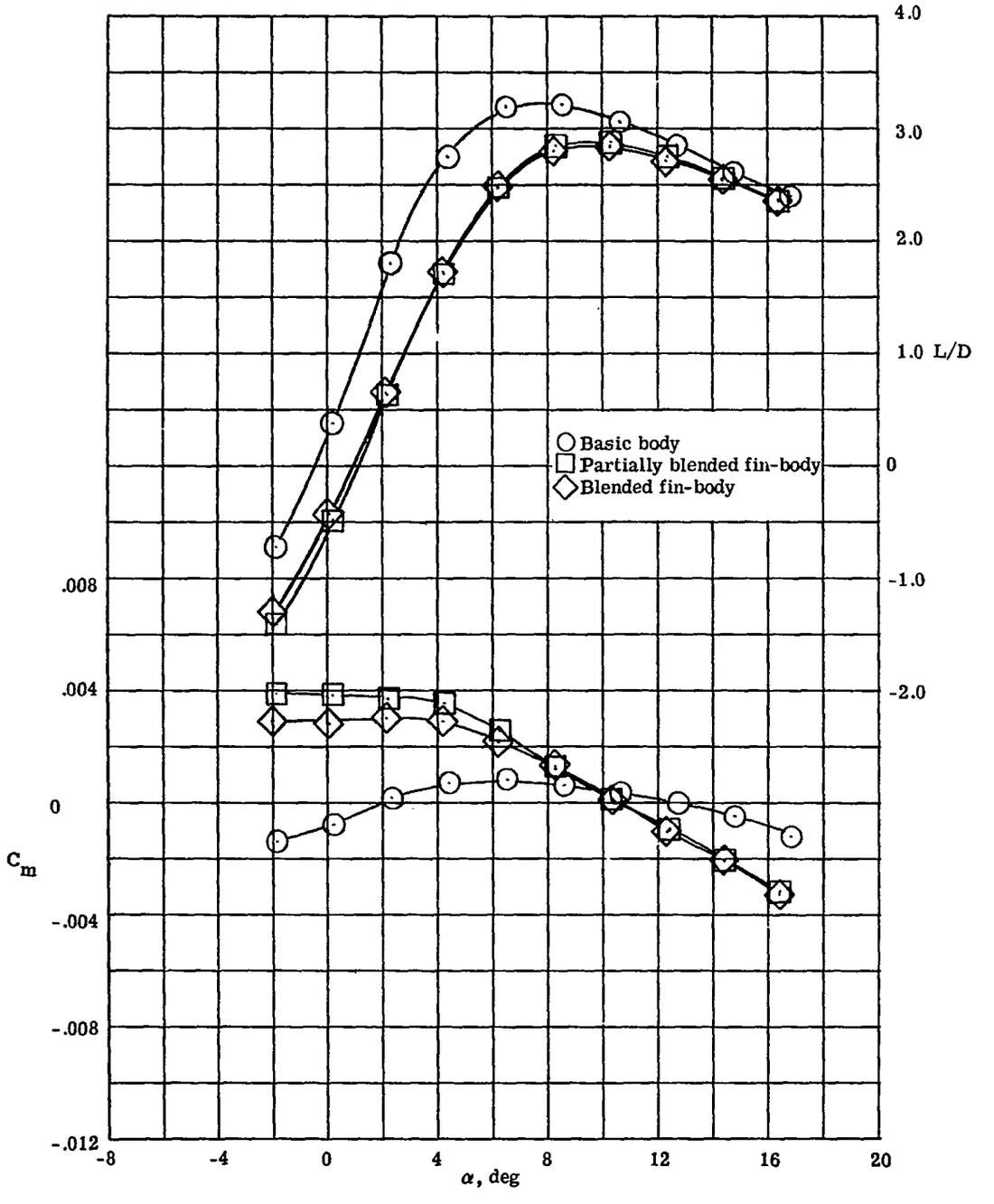

(b) Lift-drag ratio and pitching-moment coefficient.

Figure 12.- Continued.

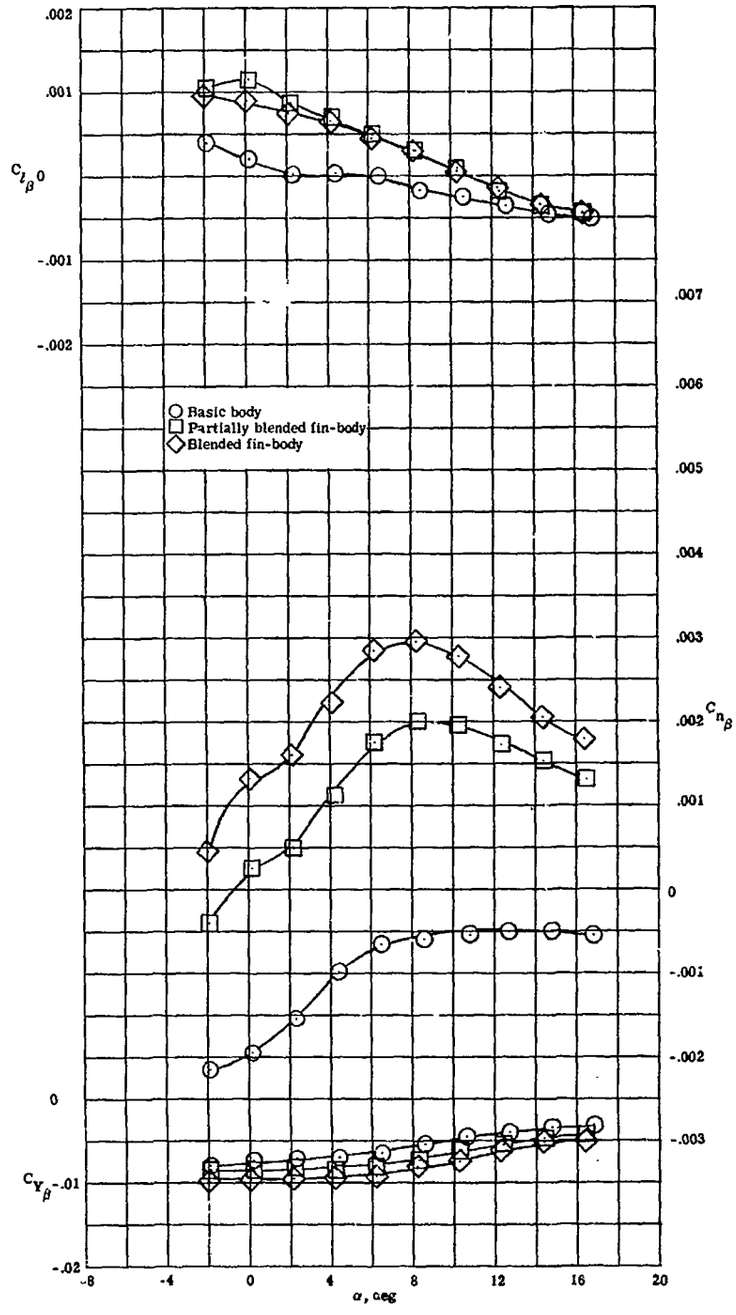

(c) Directional and lateral stability parameters.

Figure 12.- Concluded.

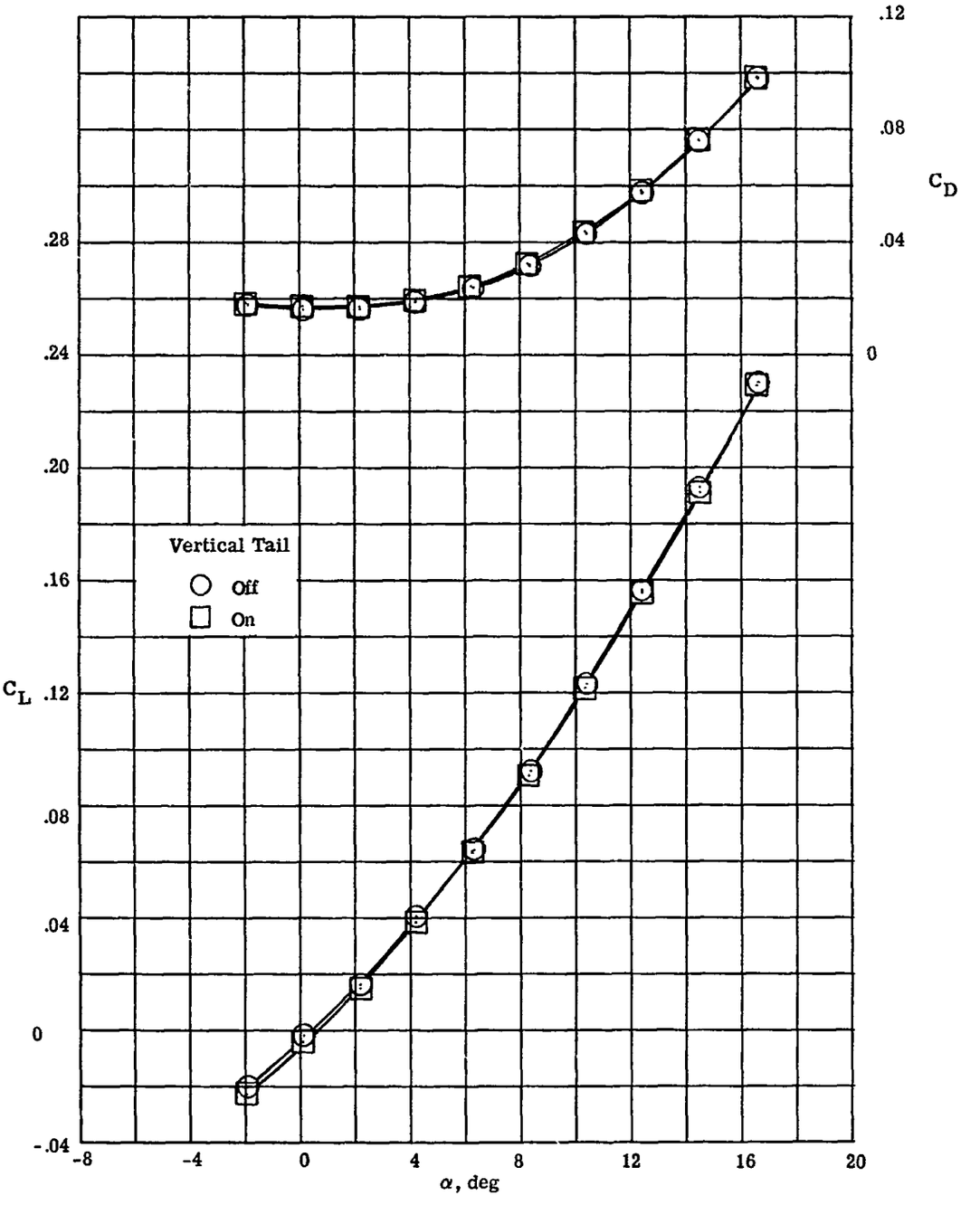

(a) Lift and drag coefficients.

Figure 13.- Effects of vertical tail on aerodynamic characteristics of configuration DL-4F. $\Phi = 20^0$; $\varepsilon = 5^0$; M = 10.4; R = 4.7×10^6.

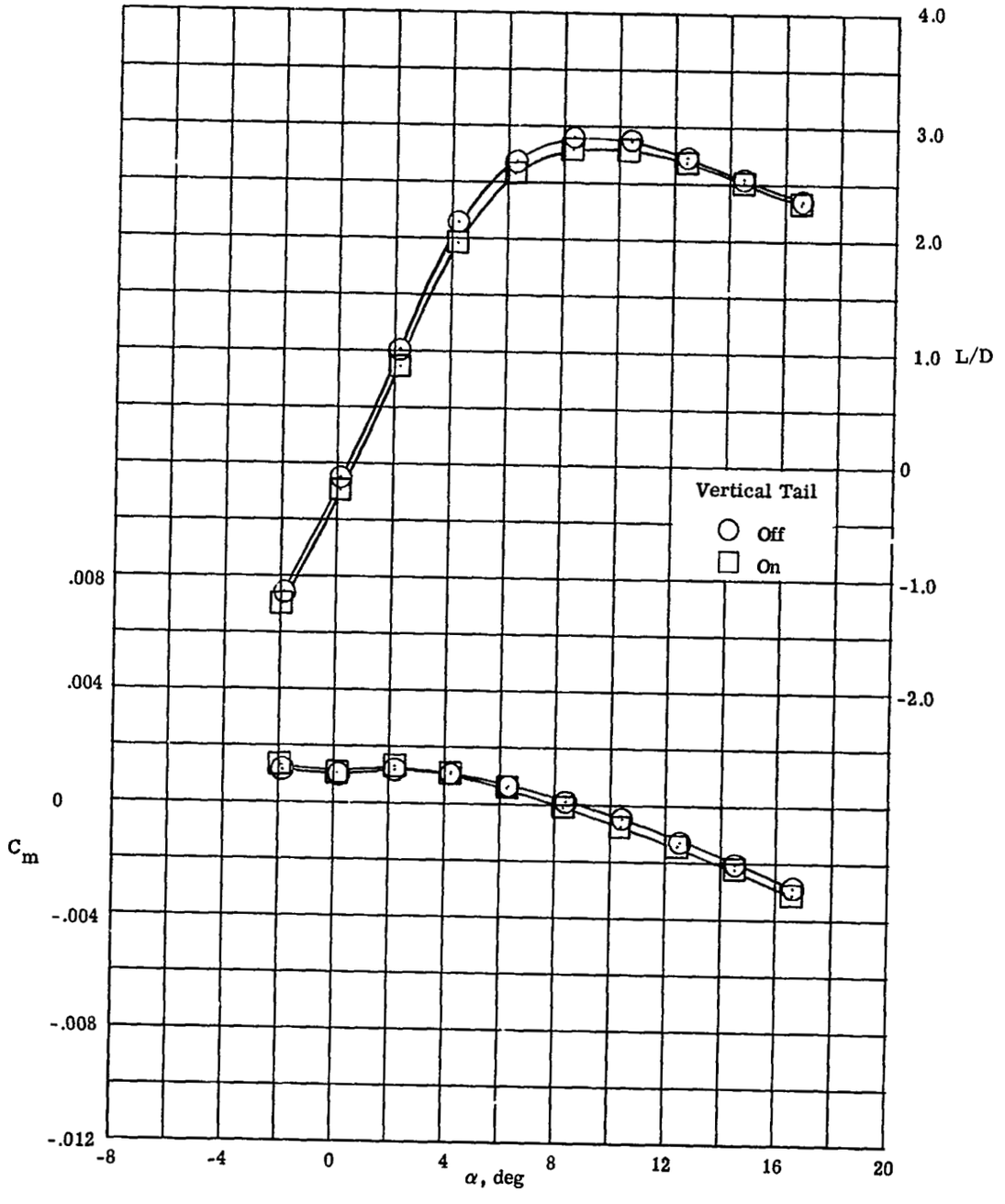

(b) Lift-drag ratio and pitching-moment coefficient.

Figure 13.- Continued.

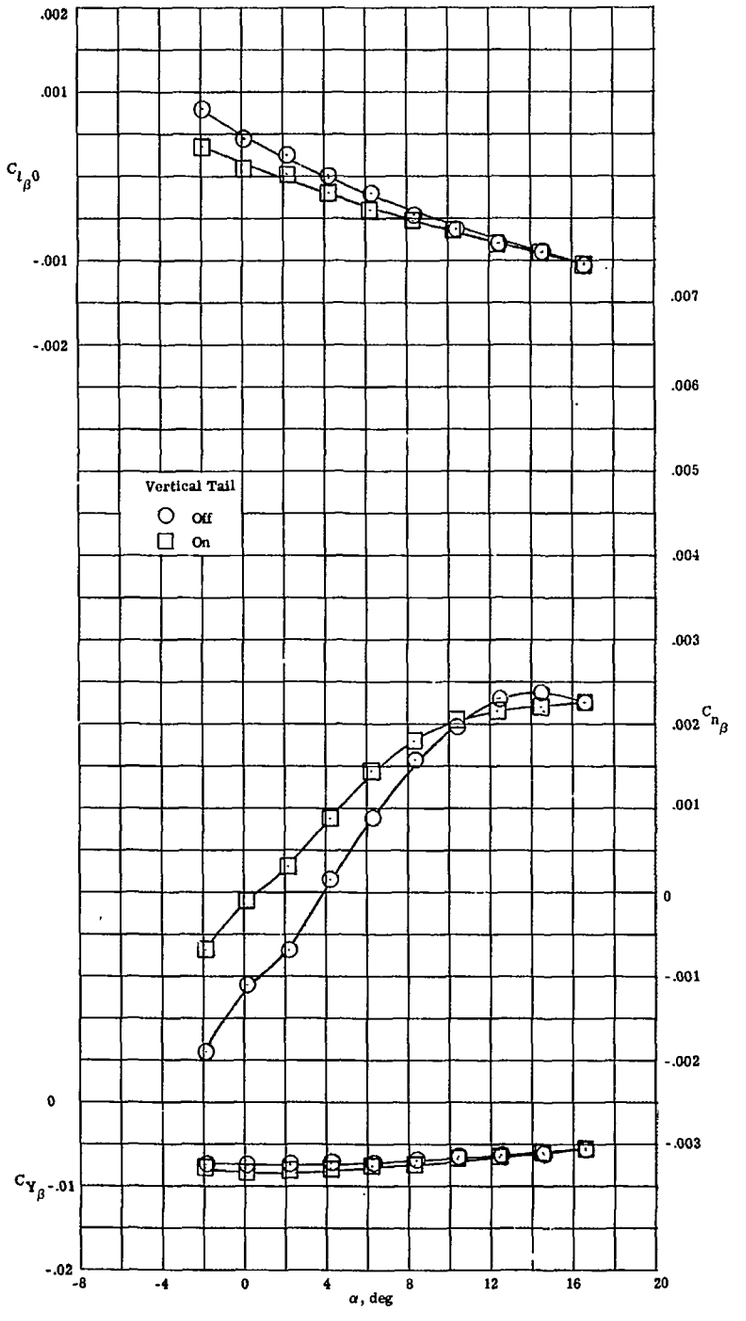

(c) Directional and lateral stability parameters.

Figure 13.- Concluded.

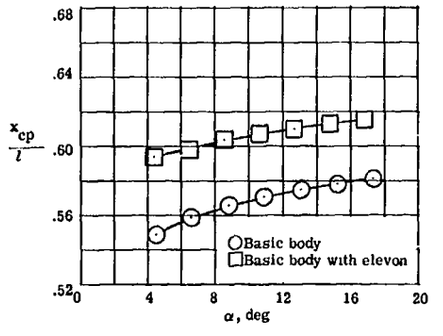

(a) Effects of addition of elevons.

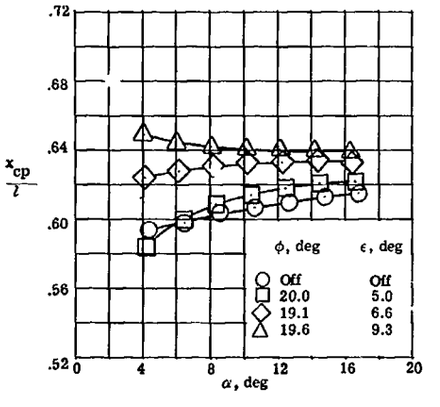

(b) Effects of tip-fin toe-in angle.

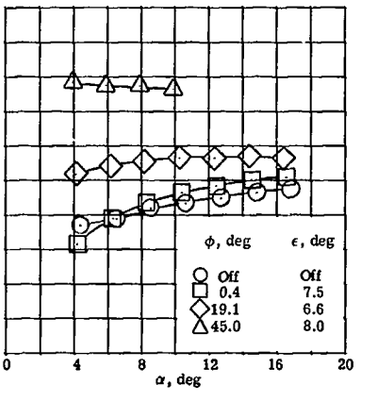

(c) Effects of tip-fin roll-out angle.

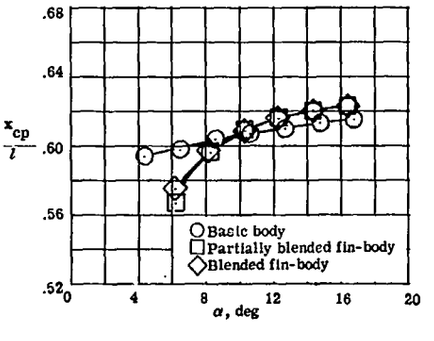

(d) Effects of aft body modification.

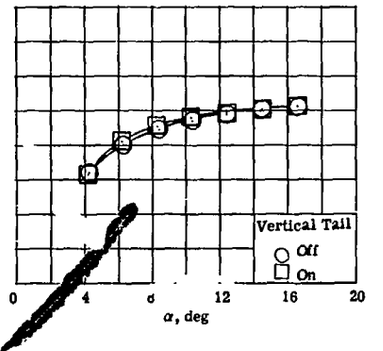

(e) Effects of addition of vertical tail.

Figure 14.- Effects of various components and modifications on center-of-pressure location. M = 10.3; R = 4.7 × 10^6.

NASA-Langley, 1970 — 1 L-6592